The Astrophysical Journal Supplement Series, 163:184–206, 2006 March
© 2006. The American Astronomical Society. All rights reserved. Printed in U.S.A.

UNDERSTANDING THE KINETICS AND DYNAMICS OF RADIATION-INDUCED REACTION PATHWAYS IN CARBON MONOXIDE ICE AT 10 K

Corey S. Jamieson,[1] Alexander M. Mebel,[2] and Ralf I. Kaiser[1,3]
Received 2005 August 3; accepted 2005 October 17

ABSTRACT

Carbon monoxide is the second most abundant molecule on icy grains in the interstellar medium. It also exists on Pluto, Triton, comets, and possibly in other icy bodies of the outer solar system like Kuiper Belt objects. With the intense radiation fields that permeate virtually all unprotected regions of space, carbon monoxide ices can be processed through energetic particle bombardment (planetary magnetospheric particles, solar wind, Galactic cosmic ray particles, and UV photons). In the present study we have investigated the effects by condensing a 1 μm layer of carbon monoxide ice on a substrate at 10 K and irradiated the sample with energetic (keV) electrons. These simulate the energetic electrons trapped in magnetospheres of planets and reproduce the irradiation effects of typical Galactic cosmic ray particles. A series of new carbon-chain (C_3, C_6) and carbon oxide species were observed including the linear isomers of C_2O, C_3O, C_4O, C_5O, $C_{6/7}O$, CO_2, C_3O_2, C_4O_2, and C_5O_2. A reaction model was proposed that outlines different reaction pathways to each of these products. Using this model, the kinetics of each route of reaction was quantified, and from this, the mechanisms and dynamics of the reactions can be understood. This work should aid in the astronomical detection of new molecular species in solar system ices as well as building up a comprehensive reaction model to describe the chemical inventory of ices on interstellar dust grains.

Subject headings: astrochemistry — comets: general — cosmic rays — infrared: ISM — ISM: molecules — methods: laboratory — molecular processes

1. INTRODUCTION

In order to accurately model reactions and molecular abundances in various regions of interstellar space, the chemistry of the carbon monoxide molecule (CO) in these environments must be fully understood. Beginning with its gas phase detection by Wilson et al. (1970) in the Orion Nebula, the carbon monoxide molecule has been shown to be abundant in the gas phase of many distinct extraterrestrial environments and has been used to characterize the physical conditions such as temperature of interstellar dust clouds (Hall et al. 1978). Carbon monoxide has also been observed in the icy mantles of interstellar dust grains (Chiar et al. 1998), the surfaces of comets (Mumma et al. 2003), and on such planetary bodies as Pluto (Grundy & Buie 2001) and Triton (Quirico et al. 1999), Neptune's largest moon.

In the solid phase, carbon monoxide is the second most abundant molecule that is condensed on dust grains in the interstellar medium (ISM), following the water molecule (H_2O; Whittet et al. 1983, 1985; Tielens et al. 1991). Since its first tentative detection in W33A in the solid state by Soifer et al. (1979) and then the confirmation by Lacy et al. (1984), solid carbon monoxide has been observed along several lines of sight in interstellar clouds including the Taurus molecular cloud (Whittet et al. 1985, 1989; Chiar et al. 1995), and the Serpens Dark Cloud (Chiar et al. 1994), as well as other protostellar objects (Geballe 1986; Ehrenfreund et al. 1997a). However, the solid state carbon monoxide abundance and distribution in different interstellar dust clouds is heavily dependent on the history (d'Hendecourt et al. 1985) and present conditions of the cloud (Tielens & Allamandola 1987). For example, the temperature of the cloud has a great effect on the ratio of carbon monoxide in the solid state versus the gas phase, which can range anywhere from very low amounts, $<1\%$ (Mithell et al. 1990), or zero to upward of 40%–50% (Whittet et al. 1985; Chiar et al. 1998). When Lacy et al. (1984) first positively identified solid carbon monoxide in the interstellar medium by its ν_1 fundamental stretching vibration that is centered at 2140 cm^{-1}, they also noticed a small shoulder located slightly lower in energy at 2135 cm^{-1}. Comparing the band shapes with laboratory work (Sandford et al. 1988; Palumbo & Strazzulla 1993; Elsila et al. 1997; Ehrenfreund et al. 1997b) it became evident that carbon monoxide exists in two distinct grain types in the interstellar medium (Tielens et al. 1991; Chiar et al. 1994; Chiar et al. 1995). The narrow feature at 2140 cm^{-1} is due to carbon monoxide in a matrix with apolar ices such as carbon dioxide (CO_2), molecular oxygen (O_2), molecular nitrogen (N_2), or other carbon monoxide molecules, while the broad 2135 cm^{-1} feature is indicative of carbon monoxide in polar ices (predominately water ice). As discussed by Chiar et al. (1994), molecular clouds will have a higher abundance of carbon monoxide on grains if they are in colder regions where there is expected to be more CO depletion (more CO condensed from the gas phase onto the interstellar dust grains), in older clouds as modeled by Ehrenfreund et al. (1992), or in clouds of greater density as modeled by Tielens & Allamandola (1987). Typically, the amount of carbon monoxide in the solid state versus water in the solid state is around 0–30% (Chiar et al. 1995). However, regions in the Serpens dark cloud (Chiar et al. 1994), young stellar objects (YSOs) in the Corona Australis complex, along with other sources (Chiar et al. 1998), show a much greater fraction of carbon monoxide ice, from 40%–60% relative to water ice. After cataloging a number of interstellar sources, Chiar et al. (1998) found that there exist three different types of interstellar dust clouds. The first group has a higher fraction of carbon monoxide in apolar ices with only a weak absorption for CO in polar ices and a total abundance of carbon monoxide compared

[1] Department of Chemistry, University of Hawai'i at Manoa, Honolulu, HI 96822; kaiser@gold.chem.hawaii.edu.
[2] Department of Chemistry and Biochemistry, Florida International University, Miami, FL 33199.
[3] Department of Physics and Astronomy, The Open University, Milton Keynes, MK7 6AA, UK.

to water ($CO/H_2O \times 100\%$) of >25%. The second group usually has equal amounts of carbon monoxide on apolar and polar grains where the percentage of CO/H_2O is 0–20%. The last group contains embedded objects where no carbon monoxide has been detected. It appears to have been sublimed by elevated temperatures. For some YSOs in group II (W33A, Mon R2 IRS 2, ρ Oph-Elias 29, Elias 32, WL5, WL12), the nonpolar interstellar dust grains can only be compositionally modeled using greater than 90% CO, meaning that there exist icy grains in some regions of the ISM containing almost pure carbon monoxide.

High abundances of carbon monoxide are also found in comets. Recent observations have shown carbon monoxide to have similar abundances relative to water as on typical grains of the interstellar medium (0–30%). Mumma et al. (2003) recorded the CO/H_2O ratios for five comets and found the values to lie between 1%–17% relative to the abundance of water. In another observation (Feldman 1986), a ratio of 20%–30% was derived for comet West (1976 VI).

Carbon monoxide has also been observed on the icy surfaces of Pluto (Grundy & Buie 2001) and Triton (Quirico et al. 1999), Neptune's largest moon. Although carbon monoxide makes up only 0.15% and 0.05% of their surfaces, respectively, their compositions could give insight to the makeup of other bodies of similar evolutionary history of the outer solar system like the Kuiper Belt objects (KBOs). With surface temperatures of 40 K (Tryka et al. 1994) and 38 K (Tryka et al. 1993) for Pluto and Triton, respectively, the low abundance of carbon monoxide could be explained by its high vapor pressure at these temperatures. Also, the radiation environment that these bodies are exposed to in the solar system could destroy the carbon monoxide molecule, forming complex products such as carbon dioxide or methanol (Moore et al. 2003). However, even though a variety of ices are expected to be found on the KBOs, water is the only molecule that has been positively identified in the rather featureless spectra of the surfaces of these bodies (Cruikshank & Dalle Ore 2003).

Nevertheless, carbon monoxide exists in a wide range of low-temperature astronomical environments, often times in high abundances. With the persistent radiation fields that exist throughout space, carbon monoxide can be chemically processed to ultimately yield new molecules. This radiation usually comes in the form of energetic ion irradiation or UV photolysis that can originate from a variety of radiation sources like magnetospheric radiation, solar/stellar radiation, or Galactic cosmic rays. Planetary bodies with a magnetic field (Earth and the outer gaseous planets) can trap ionized particles in an orbit within the magnetosphere (the torus). These particles can originate from captured solar wind ions or from the atmospheres or surfaces of bodies within the magnetosphere where neutral particles can subsequently be ionized. The density of ions orbiting within the magnetosphere is rather high, 0.1 ion cm^{-3} at Triton's orbit compared with a density of 0.005 ion cm^{-3} resulting from the solar wind (Johnson 1990). This predicts a much higher degree of radiation-induced chemistry for satellites that orbit within the radiation belt of a magnetosphere since the magnetospheric particles and solar wind particles are of similar energies (in the keV range). However, since this effect only initiates chemistry on bodies orbiting within a magnetosphere, it is dismissible for all regions related to carbon monoxide chemistry except for Triton. As an interesting aside, carbon monoxide is present on both Triton and Pluto yet only on Triton has carbon dioxide been detected. This could be due to a higher rate of carbon monoxide conversion to carbon dioxide, as illustrated by Loeffler et al. (2005), with the greater amount of radiation Triton receives in the form of magnetospheric particle bombardment.

Solar radiation is a very important for affecting chemistry within a solar system and for the astronauts that leave the protection of Earth's atmosphere. It is due to the continuous expansion of the solar corona and is composed of a photon flux as well as ions and electrons that make up the solar wind. The majority of the ions in the solar wind within our solar system are protons (96%), where helium nuclei (4%) and heavier atomic nuclei make up the balance. At the average orbiting distance of the Earth from the Sun, one astronomical unit (AU), the ion number density is 4.5 cm^{-3}. However, treating the Sun as a point source, the intensity of the solar radiation drops with an r^{-2} dependence. It is still being investigated whether the solar radiation field plays an important role in radiation-induced chemistry of ices for bodies in the deep reaches of the outer solar system. (Yeghikjan & Kaiser 2005).

The most important type of radiation for influencing chemistry in carbon monoxide ices is Galactic cosmic ray (GCR) bombardment. Cosmic rays permeate the Galaxy as a continual high-energy radiation source. They are thought to originate from remnants of supernova explosions that are accelerated to high energies by magnetic fields as they travel through the Galaxy. Like the solar wind, GCRs are composed of ions and electrons where the ions carry the majority of the energy (Simpson 1983). Ions of Galactic cosmic rays are composed of 85% protons, 12% helium nuclei; the rest are heavy nuclei. The energy distribution maximum of these ions is much higher than for the solar wind, on the order of tens of MeV (Cooper et al. 2003) for GCR ions compared to one keV for the solar wind ions. There is also an internal photon flux associated with Galactic cosmic rays inside of molecular clouds (Sternberg et al. 1987; Cecchi-Pestellini & Aiello 1992). Even though the intensity is high, the penetration depth of photons in an ice surface is on the order of less than tens of nanometers. Therefore, when considering solar induced chemistry inside the ices of cometary nuclei, Pluto or Triton, or chemistry within the surfaces of icy interstellar dust grains, only ion radiation effects need to be considered, where the penetration can be meters deep.

While there have been many experiments that investigated irradiation effects on carbon monoxide ices (§ 4.1), there still has been no study that is complete in its analysis of the products; also, the dependence of the product distributions of important physical parameters like temperature, irradiation source (keV electrons and ions vs. photons), the kinetic energy and flux of the irradiating particles, and the chemical composition (neat carbon monoxide ices vs. mixtures) have not been studied systematically. The present paper is the first in a series to investigate the radiation-induced chemistry of carbon monoxide ices at distinct physico-chemical conditions. Here it is our intent to compile a more thorough list of products observed after irradiation with energetic electrons at 10 K and to understand the mechanisms and kinetics associated with reactions to the various products.

2. EXPERIMENTAL

The experiments were carried out in a contamination free ultrahigh vacuum (UHV) stainless steel chamber; see Figure 1 (Bennett et al. 2004). The chamber can reach pressures down to 5×10^{-11} torr by use of a magnetically suspended turbo molecular pump (TMP) that is backed by a scroll pump. All pumps used are oil-free to ensure no hydrocarbon contaminants enter the system. Temperatures of 10 K are reached using a two-stage closed-cycle helium refrigerator that is interfaced directly to a polished single crystal silver mirror onto which the ices are condensed. The silver substrate is suspended by a differentially pumped rotatable feedthrough, which aligns the wafer in the

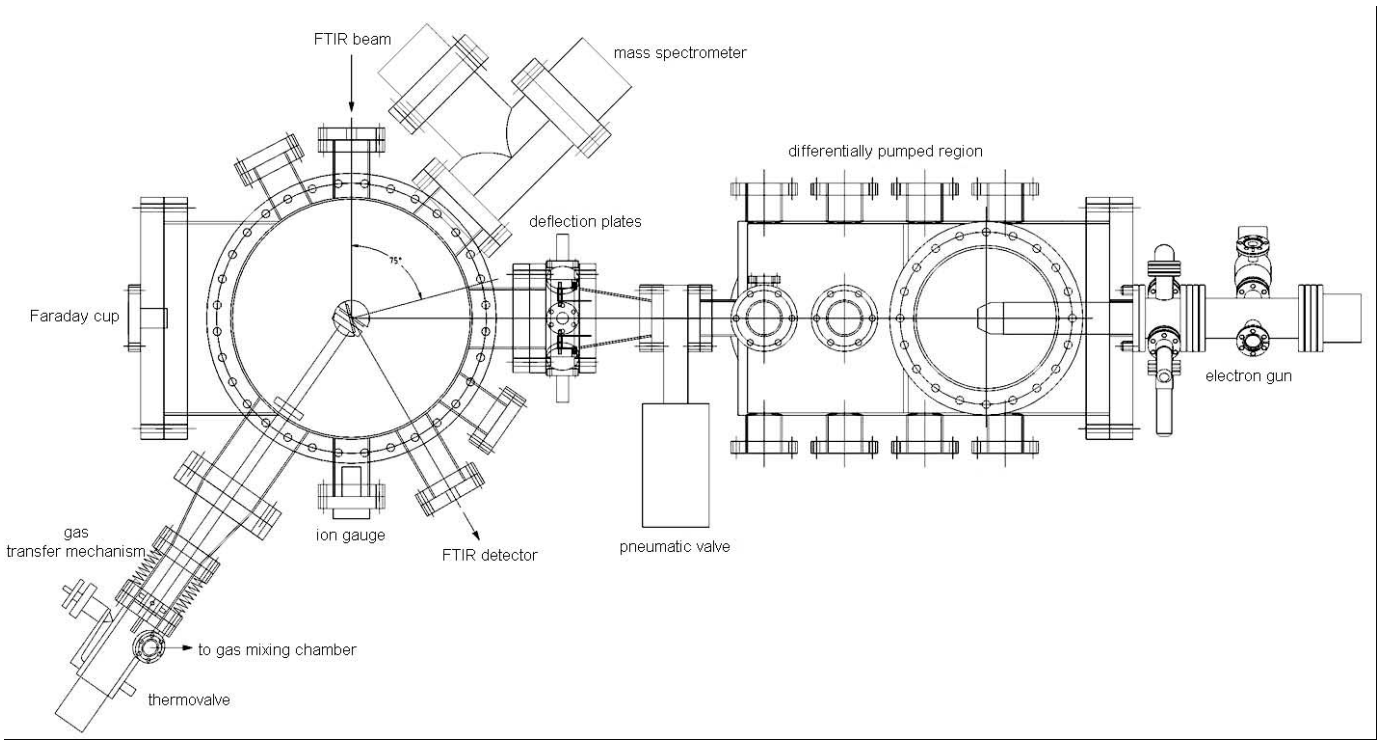

FIG. 1.—Schematic view of the experimental setup.

center of the main chamber. Gas condensation is carried out at 10 K, where the pressure is regulated by a Balzers UDV 235 thermovalve that lets gas through the linear transfer mechanism and to the gas capillary array (GCA), which evenly disburses the gas. The GCA approaches to within 5 mm of the mirror during condensation.

For this experiment, carbon monoxide gas was condensed for 3 minutes at a pressure of 5.5×10^{-7} torr at 10 K. The unirradiated spectrum was recorded (Fig. 2) using a Nicolet 510 DX Fourier transform infrared spectrometer (FTIR). Band assignments are given in Table 1. The spectrometer has a range of 6000–500 cm^{-1} and operates in absorption-reflection-absorption mode with a reflection angle of 75° from the normal relative to the mirror surface. The infrared spectra of the ice were recorded online and in situ at an integrated time of 2.5 minutes and at a resolution of 2 cm^{-1}.

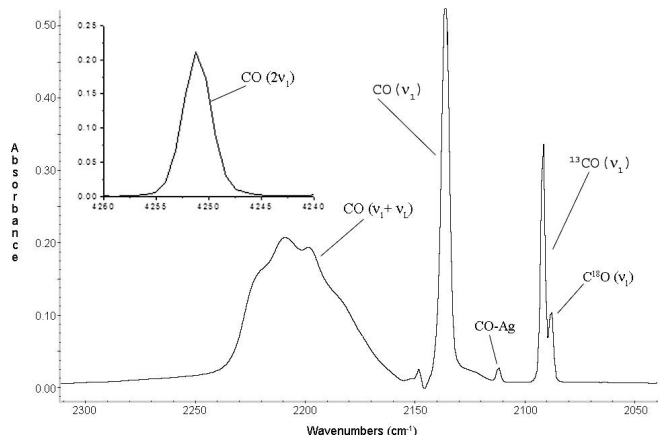

FIG. 2.—Infrared spectrum of unirradiated carbon monoxide ice at 10 K from 2300 to 2050 cm^{-1}. Due to the thickness of the sample, a partial reflectance spectrum is seen that interferes with the fundamental carbon monoxide vibration (2136 cm^{-1}).

Column densities of the molecules were calculated according to Bennett et al. (2004). The calculated column density of carbon monoxide was $(2.28 \pm 0.01) \times 10^{18}$ molecules cm^{-2}. Using the column density, the molecular weight, 28 g mol^{-1}, and the density, 1.0288 g cm^{-3} (Jiang et al. 1975a), the thickness for the carbon monoxide ice was calculated to be 1.03 ± 0.01 μm.

The ice was irradiated isothermally with 5 keV electrons to simulate the irradiation effects resulting from cosmic ray ion bombardment of an extraterrestrial ice. In our experiment, the implanted electrons were found to have an average penetration of 530 nm in the ice. This result was calculated using the "Monte Carlo simulation of electron trajectory in solids" (CASINO) program.[4] This yields an average linear energy transfer (LET) of 9.4 ± 0.4 keV μm^{-1}, which has an equivalent linear energy transfer as a 3.5 MeV proton. As later discussed in § 4.1, 99.95% of the energy from a 3.5 MeV proton is transferred to the target molecules by electronic interaction, as is the energy from the electrons in our experiment. The electron beam was operated at a nominal

[4] See http://www.gel.usherb.ca/casino/index.html.

TABLE 1

OBSERVED PEAK POSITIONS AND ASSIGNMENTS IN THE INFRARED SPECTRUM (6000–500 cm^{-1}) OF THE PURE ICE SAMPLE OF CARBON MONOXIDE AT 10 K BEFORE IRRADIATION

Frequency (cm^{-1})	Assignment
4251	CO ($2\nu_1$)
2208	CO ($\nu_1+\nu_L$)
2136	CO (ν_1)
2112	CO-Ag
2091	^{13}CO (ν_1)
2088	$C^{18}O$ (ν_1)

current of 100 nA with an extraction efficiency of 78.8% and scanned over the sample area (3.0+0.4 cm^2) to avoid heating the ice. The sample was irradiated for 1 hr, which exposed the target to 1.8×10^{15} electrons; higher beam currents were avoided to eliminate overlapping electron trajectories and heating the ice surface (Bennett et al. 2004).

3. RESULTS

3.1. *Qualitative Analysis*

The analysis of the ice sample was carried out using the FTIR spectrometer. By comparing the peak positions in the spectra with published experimental and theoretical studies, the carrier to each absorption feature was assigned. A complete listing of the molecular species present at the end of 1 hr of irradiation time along with their observed vibrational frequencies and absorption coefficients is shown in Table 2. The vibrational frequencies and the integrated absorption coefficients of various molecular species relevant to this work were calculated for comparison with literature values (Appendix A). It should be noted that there is a disparity between the theoretically calculated (gas phase) vibrational frequencies and the solid state values due to near-neighbor interactions within the ice of about 10%–20%. In comparison with known vibrational frequency assignments, a range of scaling factors of 0.93–0.97 was found to be appropriate in this investigation. This correction is acceptable for solid state vibrational frequencies as compared to the gas phase values calculated at the B3LYP/6-311G(d) level of theory.

Before irradiation, the only molecule present in the sample was carbon monoxide. Six absorptions were identified, the fundamental stretching peak (ν_1) centered at 2136 cm^{-1}, the fundamental plus lattice vibration combination band ($\nu_1+\nu_L$), 2208 cm^{-1} peak, the first overtone of the fundamental ($2\nu_1$) at 4251 cm^{-1}, the ^{13}C peak of the CO fundamental (ν_1) at 2091 cm^{-1}, and the $C^{18}O$ peak at 2088 cm^{-1}. One additional peak lies at 2112 cm^{-1}, which results from the vibrations of carbon monoxide molecules that are chemisorbed to the substrate. The C—O bond is weakened due to a back-donating charge transfer from the silver substrate to the antibonding $2\pi^*$ CO orbital resulting in a weaker energy of vibration (Froben et al. 1996). After irradiating the carbon monoxide ice for 1 hr, a series of new peaks were observed in the infrared spectrum (Figs. 3, 4, 5, and 6). In these figures, the infrared spectrum after irradiation ($t = 60$ minutes) was compared with the pure carbon monoxide spectrum ($t = 0$ minutes) for different spectral regions. A series of new carbon oxide species were identified including $C_2O(X\,^3\Sigma^-)$, $C_3O(X\,^1\Sigma^+)$, $C_4O(X\,^3\Sigma^-)$, $C_5O(X\,^1\Sigma^+)$, $C_6O(X\,^3\Sigma^-)$/$C_7O(X\,^1\Sigma^+)$ (tentative), $CO_2(X\,^1\Sigma_g^+)$,$C_3O_2(X\,^1\Sigma_g^+)$, $C_4O_2(X\,^3\Sigma_g^-)$, and $C_5O_2(X\,^1\Sigma_g^+)$, as well as carbon-chains $C_3(X\,^1\Sigma_g^+)$ and $C_6(X\,^3\Sigma_g^-)$. The structures and bond lengths of these molecules are given in Figure 7. Note that all species identified are the linear isomers.

The observed products can be generally broken up into three categories: the cummulene-like C_nO species, the C_nO_2 species, and the carbon-chain C_n species. First, we will investigate the observed C_nO molecules ($n = 2-7$) that resulted from irradiation of the carbon monoxide ice. The ν_1 vibration of the dicarbon monoxide molecule (C_2O) that was detected at 1988 cm^{-1} was observed to saturate at very low irradiation doses. This peak assignment corresponds well with our unscaled theoretically calculated frequency (2034 cm^{-1}) as well as that by Zengin et al. (1996; 2038 cm^{-1}). It also falls within the matrix-dependent range of values reported by Jacox et al. (1965) of 1978–1989 cm^{-1}. There is also a less intense peak that is seen to the lower energy side of the 1988 cm^{-1} C_2O peak at 1981 cm^{-1}. The temporal development of this band matches that of the 1988 cm^{-1} dicarbon monoxide band, and so the 1981 cm^{-1} feature can be explained by the ν_1 vibration of a C_2O molecule that exists in a different matrix site or electronic environment. The tricarbon monoxide (C_3O) molecule was identified by its ν_1 vibration centered at 2249 cm^{-1} along with the ν_2 vibration at 1913 cm^{-1}. These values compare well with the matrix isolation values reported by Brown et al. (1985a), where our values are only a few wavenumbers higher resulting from a different matrix ice. The ν_2 feature of tricarbon monoxide was found to have an overlapping absorption with the tetracarbon monoxide (C_4O) molecule as seen in Figure 5. The ν_2 vibration of the C_4O molecule was determined to be responsible for the 1919 cm^{-1} absorption, which matches the values that were experimentally found by Maier et al. (1988) and Trottier & Brooks (2004). The pentacarbon monoxide (C_5O) molecule was tentatively assigned to absorb at 2251 cm^{-1} in a water ice matrix by Dibben et al. (2000). However, this absorption is unobserved in the current experiment because it overlaps with the very intense absorptions of C_3O (2249 cm^{-1}) and C_3O_2 (2242 cm^{-1}). The only other experimental detection of C_5O was in the microwave spectral region (Ogata et al. 1995), and therefore, calculated values are necessary to compare with the infrared frequencies detected in this experiment. Two absorptions of C_5O were observed including the ν_2 peak detected at 2106 cm^{-1} and the ν_3 peak at 1817 cm^{-1}. After the theoretically calculated values (Table 1) for C_5O are scaled, there is good agreement with the observed frequencies. Other evidence that supports these assignments to C_5O is the similar slow temporal developments of the 2106 and 1817 cm^{-1} bands suggesting that a single, high-order molecule is responsible for both absorption features. Also, the intensities of the bands are comparable owing to the fact that they are calculated to have similar absorption coefficients for C_5O. A possible detection of C_6O and/or C_7O can be made based on an unassigned absorption at 2061 cm^{-1}. The most intense, unobscured vibrations of these molecules were calculated in this work to be 2146 and 2140 cm^{-1}, respectively, with IR intensities of 4.3×10^{17} and 3.7×10^{16} cm $molecule^{-1}$. After scaling these theoretical values, there is good agreement with the peak observed at 2061 cm^{-1} and the temporal evolution of the peak also seems in accordance with a higher order product; however, it is unclear whether the peak should be assigned to C_6O and/or C_7O.

Next, we will investigate the C_nO_2 molecular species that were observed in this experiment ($n = 1$, 3–5). Carbon dioxide (CO_2) was readily observed once irradiation started, evident by its intense ν_3 absorption at 2346 cm^{-1}. Other assignments for carbon dioxide included 3707 ($\nu_1+\nu_3$), 3602 ($2\nu_2+\nu_3$), 660 (ν_2), as well as the ν_3 vibration of the ^{13}C isotope of carbon dioxide identified at 2281 cm^{-1} and the $OC^{18}O$ isotope found at 2330 cm^{-1}. These values are in close agreement with the assignments given by Gerakines et al. (1995). A band centered at 1273 cm^{-1} was also assigned to carbon dioxide. This weak feature results from a splitting of the nearly degenerate ν_1 and $2\nu_2$ bands; an effect called Fermi resonance. There exists similar orbital symmetry elements that are common to both vibrations and, therefore, mixing of these bands is forbidden by perturbation theory. This gives rise to two distortion frequencies, $\nu_+ = 1383$ cm^{-1} and $\nu_- = 1276$ cm^{-1}, as studied by Gale et al. (1985) and Falk (1987). Both features were observed by our lab in previous experiments with carbon dioxide ice but only the lower energy band was observed in the current study. Carbon suboxide was easily identified, confirmed by at least nine absorptions. This includes assignments at 3070 cm^{-1} ($\nu_2+\nu_3$), 2399 cm^{-1} ($\nu_2+\nu_4$), 2242 cm^{-1} (ν_3), 2194 cm^{-1} (ν_1), 1563 cm^{-1} (ν_4), 577 & 551 cm^{-1} ($\nu_6+\nu_L$), 558 cm^{-1} (ν_5), and 542 cm^{-1} (ν_6). An absorption feature located at 2078 cm^{-1} was

TABLE 2

OBSERVED PEAKS IN THE INFRARED SPECTRUM AFTER 1 hr OF IRRADIATION, BAND ASSIGNMENTS, AND COMPARISON WITH VIBRATIONAL FREQUENCIES FROM THE LITERATURE

Assignment	Vibration	Observed Frequency (cm^{-1})	Observed Frequency (μm)	Literature Value (cm^{-1})	Absorption Coefficient (cm $molecule^{-1}$)	Reference
CO.....	$2\nu_1$	4251	2.35	4252	1.6E−19	Gerakines et al. (2005)
				4253		Vetter et al. (2000)
CO_2.....	$\nu_1+\nu_3$	3707	2.70	3708	1.4E−18 [b]	Gerakines et al. (1995)
				3708	2.6E−18	Hudgins et al. (1993)
CO_2.....	$2\nu_2+\nu_3$	3602	2.78	3600	4.5E−19 [b]	Gerakines et al. (1995)
				3600	7.9E−19	Hudgins et al. (1993)
C_3O_2	$\nu_2+\nu_3$	3070	3.26	3043	6.0E−18[b]	Gerakines & Moore (2001)
				3035		Hayden Smith & Leroi (1966)
C_3O_2	$\nu_2+\nu_4$	2399	4.17	2396	8.0E−18[b]	Gerakines & Moore (2001)
				2400		Hayden Smith & Leroi (1966)
CO_2.....	ν_3	2346	4.26	2343	7.6E−17[b]	Yamada & Person (1964)
				2436[a]	1.0E−16	This work
				2342	1.4E−16	Hudgins et al. (1993)
$OC^{18}O$	ν_3	2330	4.29			Falk (1987)
$^{13}CO_2$.....	ν_3	2281	4.38	2283	7.8E−17	Gerakines et al. (1995)
C_3O.....	ν_1	2249	4.45	2348[a]	2.5E−16[b]	This work
				2266[a]	1.9E−16	Moazzen-Ahmadi & Zerbetto (1995)
				2321[a]		Rienstra-Kiracofe et al. (2000)
				2243		Brown et al. (1985a)
C_3O_2	ν_3	2242	4.46	2411[a]	4.7E−16[b]	This work, Wang et al. (2002)
				2352	3.6E−16	Kim et al. (1998)
				2242	1.3E−17	Gerakines & Moore (2001)
				2255		Hayden Smith & Leroi (1966)
C_5O_2	ν_2	2211[c]	4.52	2213		Maier et al. (1988)
CO.....	$\nu_1+\nu_L$	2208	4.53	2208		Ewing & Pimentel (1961)
C_3O_2	ν_1	2194	4.56	2274[a]	Inactive	This work, Wang et al. (2002)
				2179		Kim et al. (1998)
				2196		Carreira et al. (1973)
				2197		Lolck & Brodersen (1979)
				2184		Hayden Smith & Leroi (1966)
CO.....	ν_1	2136	4.68	2139	1.1E−17	Jiang et al. (1975b)
				2138		Hudgins et al. (1993)
C_4O_2	ν_2	2122	4.71	2215[a]	3.4E−16[b]	This work, Wang et al. (2002)
				2135	2.5E−16	Kim et al. (1998)
				2130		Maier et al. (1990)
CO-Ag.....	ν_1	2112	4.73	2110		Froben et al. (1996)
C_5O.....	ν_2	2106	4.75	2232[a]	1.2E−16[b]	This work
				2150[a]	5.0E−17	Moazzen-Ahmadi & Zerbetto (1995)
				2166[a]	1.1E−16	Botschwina et al. (1995)
^{13}CO	ν_1	2091	4.78	2092	1.3E−17[b]	Gerakines et al. (1995)
$C^{18}O$	ν_1	2088	4.79			
C_3O_2	$\nu_4+\nu_6$	2078	4.81			
$^{?}$		2063	4.85			
C_6O, $C_7O^{?}$.....		2061	4.85	2079 (C_6O)		Ewing (1989)
				2073 (C_6O)		Moazzen-Ahmadi & Zerbetto (1995)
				2061 (C_7O)		Moazzen-Ahmadi & Zerbetto (1995)
C_5O_2	ν_3	2059	4.86	2138[a]	7.4E−17[b]	This work, Wang et al. (2002)
				2049	7.2E−17	Kim et al. (1998)
				2059		Maier et al. (1988)
C_3	ν_3	2019	4.95	2148[a]	1.3E−16[b]	This work
				2039	1.0E−16	Hutter et al. (1994)
				2028		Gerakines et al. (1996)
				2038		Weltner et al. (1964)
C_2O.....	ν_1	1988	5.03	2034[a]	2.4E−17[b]	This work
				2038[a]		Zengin et al. (1996)
				1976		Maclagan & Sudkeaw (1993)
				1978		Jacox et al. (1965)
C_2O.....	ν_1	1981	5.05			
C_6	ν_4	1951	5.13	1972	1.3E−16[b]	Hutter et al. (1994)
				2032[a]	1.8E−16	This work
				1952		Kranze & Graham (1993)
C_4O.....	ν_2	1919	5.21	1985[a]	5.8E−17[b]	This work
				1906[a]	5.3E−17	Moazzen-Ahmadi & Zerbetto (1995)
				1990[a]		Rienstra-Kiracofe et al. (2000)
				1920		Ewing (1989)
				1922		Maier et al. (1988)

TABLE 2—*Continued*

Assignment	Vibration	Observed Frequency (cm^{-1})	Observed Frequency (μm)	Literature Value (cm^{-1})	Absorption Coefficient (cm $molecule^{-1}$)	Reference
C_3O.....	ν_2	1913	5.23	1974[a]	5.7E−18[b]	This work
				1887[a]	3.5E−18	Moazzen-Ahmadi & Zerbetto (1995)
				1972[a]		Rienstra-Kiracofe et al. (2000)
				1907		Brown et al. (1985a)
C_5O.....	ν_3	1817	5.50	1919 [a]	6.2E−17[b]	This work
				1834[a]	5.8E−17	Moazzen-Ahmadi & Zerbetto (1995)
				1850[a]	8.0E−17	Botschwina et al. (1995)
C_3O_2	ν_4	1563	6.40	1650[a]	1.7E−17	This work, Wang et al. (2002)
				1578	1.7E−17	Kim et al. (1998)
				1581	5.0E−18	Gerakines & Moore (2001)
				1582		Hayden Smith & Leroi (1966)
CO_2.....	$2\nu_2$	1273	7.86	1276		Gale et al. (1985)
				1280		Falk (1987)
CO_2.....	ν_2	660	15.2	660, 665	1.1E−17	Gerakines et al. (1995)
				666[a]	5.4E−18	This work
C_3O_2	$\nu_6+\nu_L$	577	17.3	582		Hayden Smith & Leroi (1966)
C_3O_2	ν_5	558	17.9	596[a]	Inactive	This work, Wang et al. (2002)
				563		Kim et al. (1998)
				573		Hayden Smith & Leroi (1966)
C_3O_2	$\nu_6+\nu_L$	551	18.2	558		Hayden Smith & Leroi (1966)
C_3O_2	ν_6	542	18.4	591[a]	1.2E−17	This work, Wang et al. (2002)
				549[a]	9.8E−18	Kim et al. (1998)
				540	1.4E−18	Gerakines & Moore (2001)
				530		Hayden Smith & Leroi (1966)

NOTE.—Absorption coefficients are indicated when available.
[a] Unscaled theoretical vibrational frequencies calculated at various levels of theory (recommended scaling dependent on the level of theory).
[b] Absorption coefficient used to calculate column density of the molecule.
[c] Absorption feature only observed during warm-up phase of the experiment.
[?] Indicates tentative or unknown assignments.

also assigned to carbon suboxide. A literature reference for this band could not be found, however, the temporal evolution of the band matches those of the known carbon suboxide absorptions, so it is suggested that the 2078 cm^{-1} ($\nu_4+\nu_6$) band also belongs to C_3O_2. The vibrational mode of this band was inferred from our calculated frequencies of the fundamental vibrations. The 2122 cm^{-1} band was assigned to the very intense ν_2 vibration of the C_4O_2 molecule as previously found by Maier et al. (1990) at 2130 cm^{-1}. Using our vibrational frequency calculations, the next most intense vibration of $C_4O_2$was calculated to be 26 times weaker and would therefore be on the noise level of the experiment excluding any possibility of detection. The C_5O_2molecule was identified by the 2059 cm^{-1} feature, which exactly matches the ν_3 value reported by Maier et al. (1988). As discussed later in § 4.8, a second band was found (2211 cm^{-1}, ν_2) in the infrared spectrum during the warm-up phase of the experiment when the more volatile molecules had sublimed leaving behind the higher order carbon oxide species. This confirms the identification of C_5O_2 and the assignments compare well with the vibrational frequencies found by Maier et al. (1988).

Finally, we will present the identifications of the pure carbon-chain molecules observed (C_n, $n = 3, 6$) as a consequence of

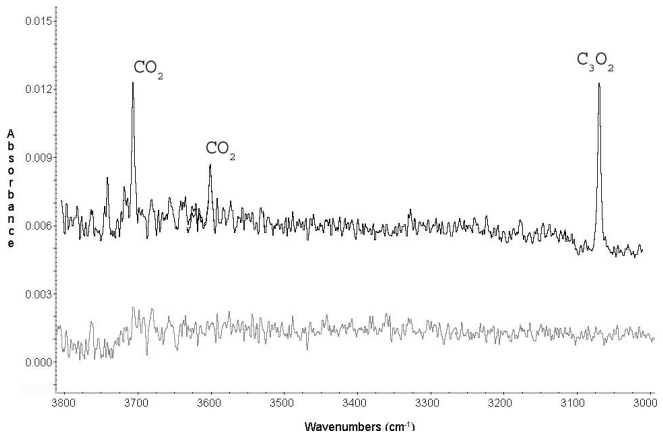

FIG. 3.—Infrared spectrum of carbon monoxide ice at 10 K before irradiation (*gray spectrum*) and after 60 minutes of irradiation (*black spectrum*) in the range of 3800–3000 cm^{-1}.

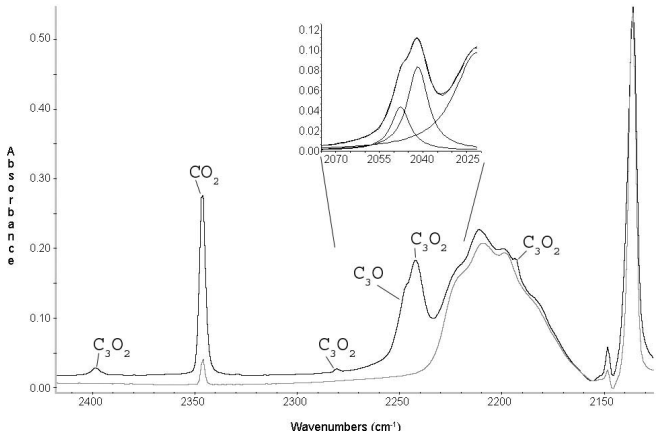

FIG. 4.—Infrared spectrum of carbon monoxide ice at 10 K before irradiation (*gray spectrum*) and after 60 minutes of irradiation (*black spectrum*) in the range of 2410–2130 cm^{-1}.

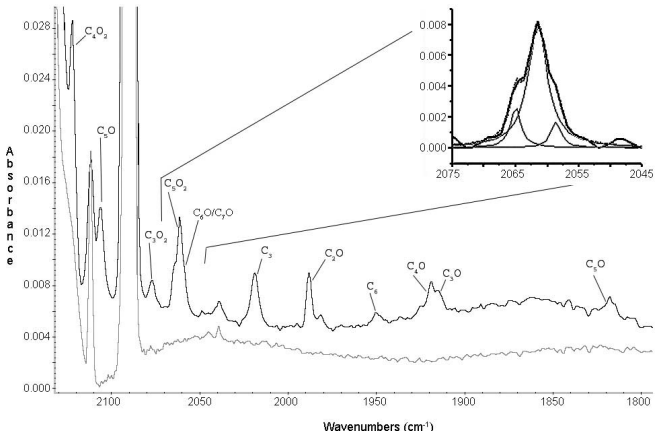

FIG. 5.—Infrared spectrum of carbon monoxide ice at 10 K before irradiation (*gray spectrum*) and after 60 minutes of irradiation (*black spectrum*) in the range of 2130–1800 cm^{-1}.

irradiation. The tricarbon (C_3) molecule was detected at 2019 cm^{-1}(ν_3), which is 10–20 cm^{-1}, lower in energy than previous experimental investigations have found, as indicated in Table 1. When comparing the C_3 assignment found at 2028 cm^{-1} in the experiment by Gerakines et al. (1996) investigating UV irradiation on CO ice, the nearest absorption in the current experiment is the relatively intense 2019 cm^{-1} band. Even though the same matrix ice was used (carbon monoxide), a shift in the vibrational frequency can still take place due to a number of factors like condensation rate or substrate surface, which can affect the crystal structure of the carbon monoxide matrix, impurities, sample thickness, and sample temperature. Also, as mentioned in § 4.6, the 2019 cm^{-1} band exhibits kinetics that belong to a molecule that has a multistep synthesis, which should be expected for C_3. Finally, an absorption feature that did not develop to a detectable intensity until almost two-thirds of the way through the 1 hr irradiation phase was the 1951 cm^{-1} band (§ 4.6). The great amount of time before the band is observed indicates that the molecule responsible for this absorption is produced in a high-order multistep synthesis and/or by kinetically slow reactions. A comparison of the matrix isolation value of C_6 at 1952 cm^{-1} (Kranze & Graham 1993) matches the observed band position in the current experiment. However, there was no indication that C_4 or C_5 were present in the sample. Observation of these molecules is expected to precede C_6 because C_6 is a higher order product.

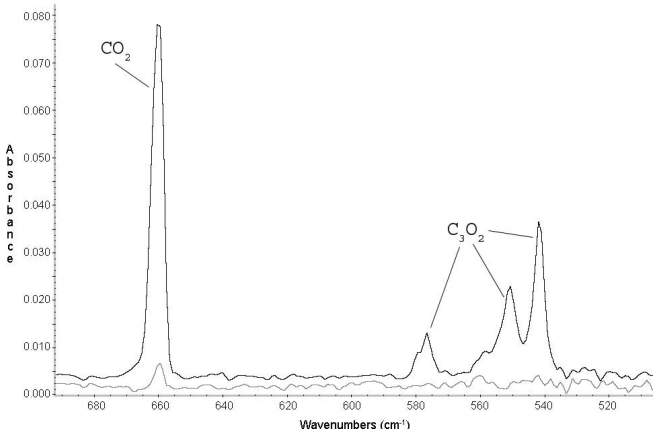

FIG. 6.—Infrared spectrum of carbon monoxide ice at 10 K before irradiation (*gray spectrum*) and after 60 minutes of irradiation (*black spectrum*) in the range of 690–510 cm^{-1}.

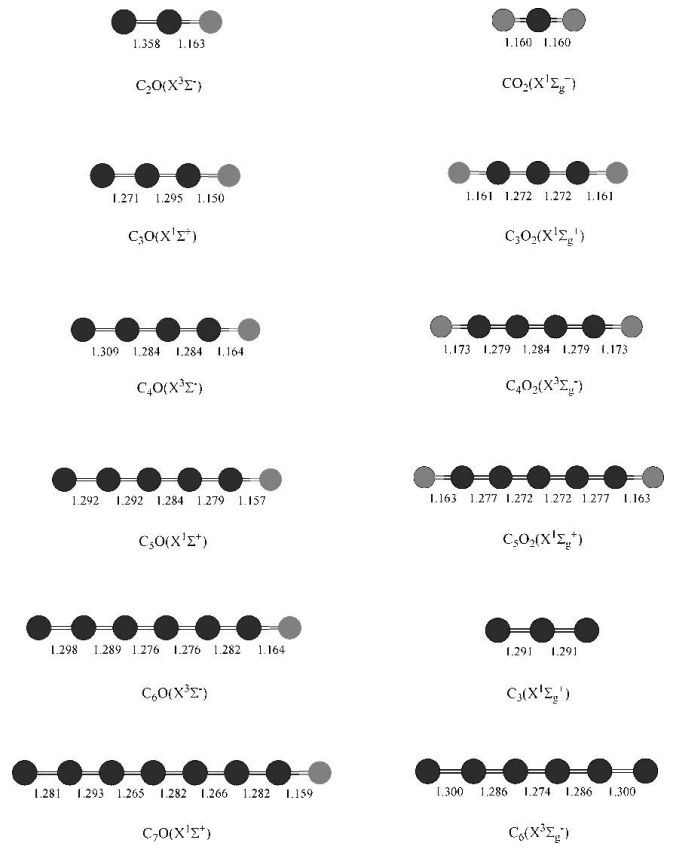

FIG. 7.—Geometries and bond lengths of molecules resulting from the 1 hr irradiation of carbon monoxide ice are shown.

From frequency calculations by Hutter et al. (1994), it appears the most intense C_4 absorption feature (1549 cm^{-1}) could be lost in the noise of the infrared spectra. On the other hand, the C_5 molecule has its most intense band (2169 cm^{-1}) obscured by the carbon monoxide fundamental and would only be observable by a low-intensity band near 1440 cm^{-1}. These considerations could explain the detection of C_6 without its two carbon-chain precursors.

3.2. *Mass Balance*

To check the consistency of our peak assignments, the total atomic carbon and oxygen abundances were compared at beginning and the end of irradiation to make sure that the mass balance was conserved. The balance should be maintained since the mass spectrometer detected no molecules leaving the sample during irradiation (§ 3.3). Using the integrated absorption coefficients for representative peaks of each molecule, the column densities after the irradiation period were calculated and are presented in Table 3 (see Bennett et al. 2004 for sample calculation). Using the column densities of the new products observed after irradiation, the total carbon and oxygen atom abundances were calculated. For carbon, $(1.07 \pm 0.03) \times 10^{16}$ atoms cm^{-2} were found in the products. For oxygen, $(1.10 \pm 0.01) \times 10^{16}$ atoms cm^{-2} were calculated in the products. However, it must be noted that we could not account for infrared inactive species such as dicarbon (C_2) molecules or the unreacted carbon atoms preserved in the cold matrix. Based on these considerations, we can conclude that within the error limits, the carbon-oxygen balance is preserved in the experiment, as expected. This also allows us to calculate the amount of carbon monoxide that was destroyed during irradiation. A direct measurement was not possible because of the well-known band-broadening effects that accompany

TABLE 3
COLUMN DENSITIES FOR THE MOLECULAR SPECIES PRODUCED AFTER 60 MINUTES OF IRRADIATION TIME

Molecule	Peak (cm^{-1})	Column Density (molecules cm^{-2})
CO_2	2346	(3.71 ± 0.01)E15
C_2O	1988	(9.2 ± 0.5)E13
C_3	2019	(5.3 ± 0.2)E13
C_3O	1913	(6.2 ± 0.8)E14
C_3O_2	2249	(1.3 ± 0.1)E15
C_4O	1919	(5.4 ± 0.6)E13
C_4O_2	2122	(3.5 ± 0.1)E13
C_5O	2106	(6.7 ± 0.2)E13
C_5O_2	2059	(3.2 ± 0.4)E13
C_6	1951	(6.4 ± 1)E12

NOTE.—The values were calculated using the integrated absorption coefficients from Table 2.

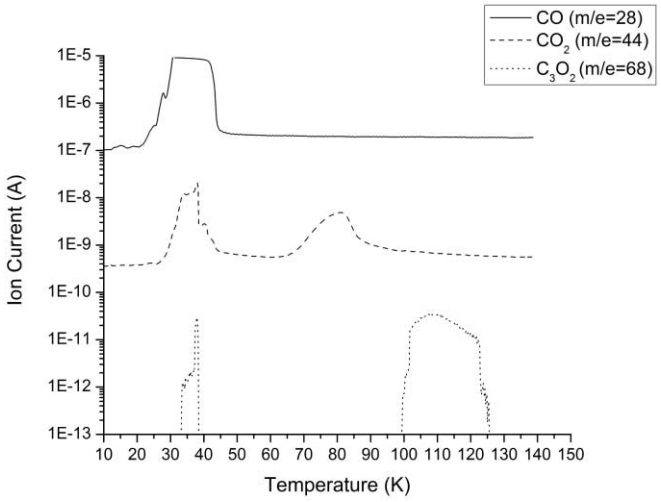

FIG. 8.—After the irradiation and isothermal phases of the experiment, the ice sample was heated at a rate of 0.5 K $minute^{-1}$. The quadrupole mass spectrometer was able to detect carbon monoxide, carbon dioxide, and carbon suboxide in the gas phase. The carbon monoxide signal saturated between 31 and 41 K.

carbon monoxide irradiation (Palumbo & Strazzulla 1993) and the change in the integrated absorption coefficients that are used to calculate column densities. Therefore, if $(1.10 \pm 0.01) \times 10^{16}$ oxygen atoms present in the products all came from destroyed carbon monoxide, then $(1.10 \pm 0.01) \times 10^{16}$ molecules of carbon monoxide would have been processed during irradiation. This means that $0.49 \pm 0.01\%$ of the carbon monoxide molecules were destroyed by the irradiation.

3.3. *Quadrupole Mass Spectrometer Analysis*

Molecules that were released into the gas phase were detected using a quadrupole mass spectrometer that was affixed directly to the main chamber. The mass spectrometer data were acquired for the duration of the experiment beginning 10 minutes before the start of irradiation, through the isothermal phase, and during the warm-up phase, until all of the molecules had either reacted to other species and/or sublimed into the gas phase to be detected.

During irradiation and for the 1 hr isothermal phase there were no molecules detected in the gas phase. This also demonstrates that the electron beam does not heat our sample surface; since our mass spectrometer is very sensitive to partial pressures as low as 10^{-15} torr, which would in turn correlate to a temperature increase of the surface of an apolar ice such as methane and carbon monoxide of 0.5 K. Consequently, we can conclude that the irradiation does not induce heating of the ice surface. Not until the sample temperature was increased were the molecules able to sublime to be detected by the mass spectrometer. The first molecule to sublime was carbon monoxide, where the majority was detected between 26 and 42 K with a maximum signal at around 37 K (Fig. 8). This correlated well with a decrease in solid state carbon monoxide as observed in the infrared spectra. The second molecule detected was carbon dioxide, which was observed to sublime between 67 and 90 K with a maximum at around 81 K in the mass spectrometer. Finally, mass-to-charge 68, corresponding to C_3O_2, sublimed at around 110 K. The increasing temperatures at which the peaks are observed, from 37 to 81 to 110 K, correlates nicely with the rising molecular weight of the subliming species. Note that during the warm-up phase, there were other masses observed in the mass spectrometer corresponding to neutral species like C, O, C_2, O_2, and C_2O. However, the same experiment was repeated except that the radiation source was never turned on to serve as a blank control. It was determined that these species resulted from fragments of higher order products like carbon monoxide, carbon dioxide, and carbon suboxide and/or ion-molecule reactions in the ionizer of the mass spectrometer and that they were not irradiation products that had sublimed into the gas phase. Note that we were unable to observed species heavier than carbon suboxide in the gas phase. This indicates that the higher order species formed such as C_5O_2 may be unstable to sublimation and may fragment or react with other species before being detected by the mass spectrometer.

4. DISCUSSION

4.1. *Nuclear versus Electronic Energy Loss*

We would like to elucidate briefly on the underlying physical effects since these considerations will help us not only to interpret our results, but also to compare our data with previous experimental investigations (Table 4). As a cosmic ray particle enters an icy body, the kinetic energy of the implant is being transferred to the target atoms. The energy transfer can be quantified in terms of the nuclear (S_n) and electronic (S_e) interaction potential. A variety of effects can take place (Kaiser 2002). Considering the energy loss via the nuclear interaction potential, which is often expressed as a screened coulomb potential between the implant and the target atom, the ion passes on part of its kinetic energy to the atoms of the ice. If this energy transfer exceeds the binding energy of the atom, the chemical bond is broken. This generates so-called primary knock-on particles (PKOs; first generation of knock-on particles). The knock-on particles can transfer their energy in consecutive encounters to the target atoms resulting in a collision cascade of secondary, tertiary, and higher knock-on atoms. Moderated to about 1–10 eV—the so-called chemical energy range—these atoms can undergo nonequilibrium chemistry via insertion, abstraction, and addition to chemical bonds. As an order of magnitude, the nuclear energy transfer dominates at kinetic energies of the implanting ion of less than about 1 keV amu^{-1}. However, cosmic ray particles have energies larger than the high keV range. Therefore, these species interact via the electronic interaction potential with the target atoms. As a matter of fact, 10 MeV protons for a typical cosmic ray ion, 99.95% of the energy will be lost via the electronic potential of the carbon monoxide molecules (Fig. 9). This result was calculated using the Stopping and Range of Ions in Matter (SRIM) program. For background

TABLE 4

PREVIOUS EXPERIMENTAL INVESTIGATIONS STUDYING THE IRRADIATION EFFECTS ON PURE CARBON MONOXIDE ICE

Study	Irradiation Source	Energy Flux (eV cm^{-2} s^{-1})	Dosage (eV cm^{-2})	Sample Analysis	Reported Products/Results
Baird (1972)	1.75 MeV H^+	1.75E18	1.25E22	IR spectroscopy	C_3O_2 polymers
Haring et al. (1984)	3 keV Ar^+	1.4E18	...	Mass spectrometer	C, O, C_2, CO, O_2, C_2O, CO_2, $(CO)_2$, C_3O_2 polymers
	3 keV He^+	1.4E18			
	6 keV H_2^+	2.8E18			
Chrisey et al. (1986)	30 keV Kr^+	7.5E16	1.2E21	Mass spectrometer	O, C_2, CO, O_2, CO_2, $(CO)_2$, C_3O_2 polymers
Gerakines et al. (1996)	6–10 eV photons	(6–10)E15	(2.2–3.6)E19	IR spectroscopy	C_3, C_2O, C_3O, CO_2, C_3O_2
Gerakines & Moore (2001)	5–11 eV photons	...	5.0E18	IR spectroscopy	CO, C_2O, CO_2, C_3O_2, and other unassigned peaks
	0.8 MeV H+		7.9E19		
Cottin et al. (2003)	UV photons	...	...	IR spectroscopy	CO destruction cross section
Trottier & Brooks (2004)	2 MeV H^+	1.2E18	4.3E21	IR spectroscopy	C_6, CO, C_2O, C_4O, CO_2, C_3O_2, C_5O_2, C_7O_2, O_3
Loeffler et al. (2005)	10.2 eV photons	1.1E16	2E19	IR spectroscopy	C_2O, CO_2, C_3O_2, C_5O_2, C_7O_2
	200 keV H^+	2E17	3.5E20		

NOTE.—A collection of references is given along with the irradiation conditions (fluxes and dosages were calculated from information given in the reference) and reported products or information resulting from the irradiation.

information on the theory of the SRIM program see Ziegler et al. (1985). Here a 10 MeV proton will penetrate to a depth of about 1.4 mm in carbon monoxide ice, where a 100 MeV proton can penetrate to 84.7 mm (Fig. 9). As the ion travels through the ice, the "electronic energy transfer" will lead to vibrational and electronic excitation as well as ionization of the target molecules. If a molecule is excited to a repulsive energy surface, simple bond ruptures can also occur producing species in either the ground or excited electronic state. Furthermore, these atoms have an excess kinetic energy (often a few eV) and are therefore not in thermal equilibrium with the surrounding 10 K target. Also, the electrons generated in the ionization process (δ electron) can leave the molecule with energies up to a few keV and initiate further vibrational and/or electronic excitation of the target molecules. Through these mechanisms, molecules within an ice will be chemically modified as bond rupture processes and recombination of radicals form new products.

There have been a number of experimental investigations that have studied the chemistry of carbon monoxide ice induced by radiation (Table 4). Using heavy ion bombardment on a carbon monoxide ice surface at low temperatures, Haring et al. (1984; 6 keV Ar^+) and Chrisey et al. (1986; 30 keV Kr^+) observed new products resulting from irradiation including carbon dioxide (CO_2) and molecular oxygen (O_2), and a dark residue that was nonvolatile at room temperature, which was attributed to carbon suboxide (C_3O_2) polymers as previously found by Baird (1972). Using ultraviolet photolysis, Gerakines et al. (1996) irradiated carbon monoxide and observed CO_2, C_2O, C_3, C_3O, and C_3O_2 as products. However, during warm-up, there was no sign of residue in the infrared spectrum, indicating that no carbon suboxide polymers had formed. This result is different from the aforementioned experiments of carbon monoxide irradiation but could be explained by different energy doses absorbed by the ice sample using UV photolysis versus ion bombardment (Gerakines et al. 2000; Gerakines & Moore 2001; Loeffler et al. 2005) and by a dominating nuclear interaction potential of the keV noble gas ions with the carbon monoxide sample, which can lead to the release of multiple free oxygen atoms by direct collisions of the implant with the carbon monoxide molecules. Also, photons interact only in single quantum processes and, hence, cannot generate collision cascades. Gerakines et al. (1996) showed that the dissociation of CO by photolysis follows a different mechanism than the nuclear energy transfer induced dissociation via ion bombardment. In photolysis a carbon monoxide molecule absorbs the radiation and is promoted to an electronically excited state (eq. [1]). The excited carbon monoxide molecule can react

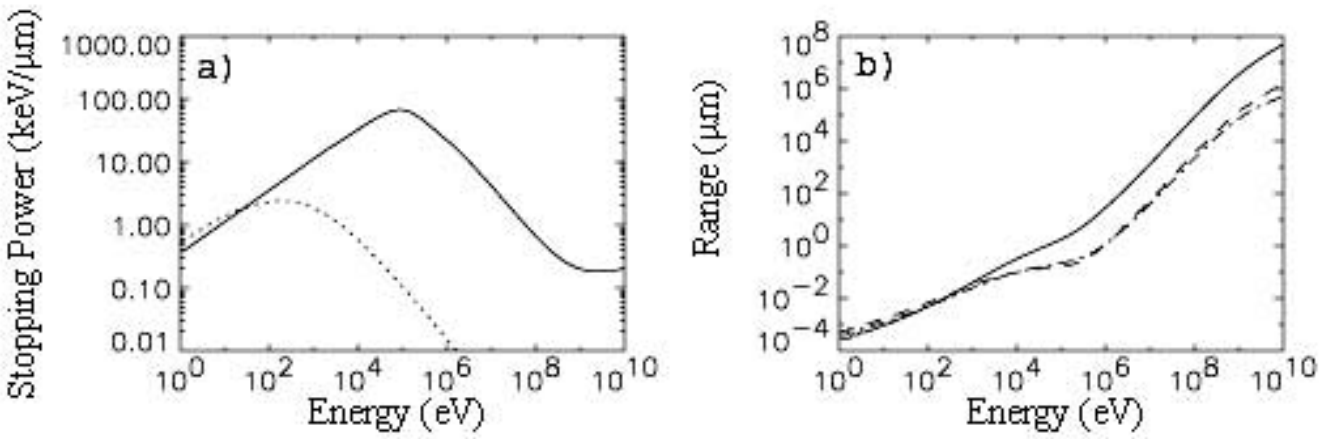

FIG. 9.—(*a*) Energy-dependent electronic (*solid*) and nuclear (*dashed*) stopping powers in solid carbon monoxide. (*b*) Projected range (*solid*), longitudinal (*dashed*), and lateral (*dash-dotted*) stragglings. The calculations were made using the SRIM program; see text for details.

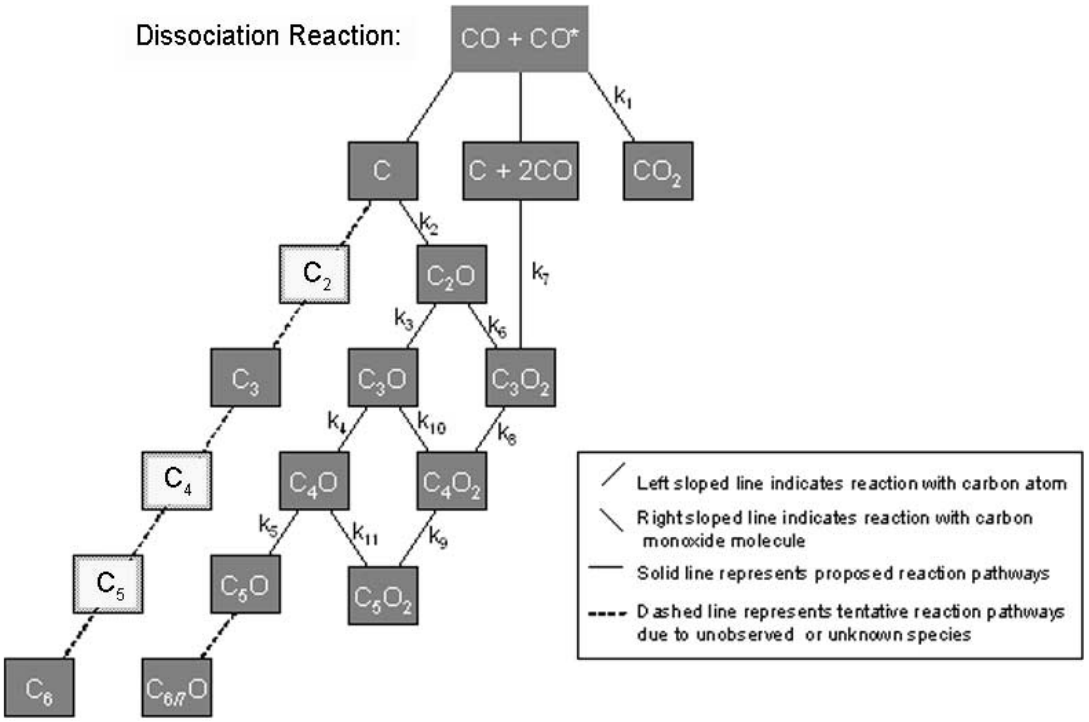

FIG. 10.—Schematic of the proposed reaction model is shown. After the initial dissociation reaction, left sloped lines indicate the molecule reacting with a carbon atom, where right sloped lines indicate reaction with a carbon monoxide molecule as mentioned in the key. The C_2, C_4, and C_5 species were unobserved and the assignment between C_6O and C_7O is uncertain. This limits the ability to understand the kinetics of some of the pathways to the observed molecules (*dashed lines*).

with a second, neighboring carbon monoxide molecule, which is still in the electronic ground state, to produce the carbon dioxide molecule plus a carbon atom (Okabe 1978):

$$\mathrm{CO}(X\ ^1\Sigma^+) \xrightarrow{h\nu} \mathrm{CO}^*, \quad (1)$$

$$\mathrm{CO}^* + \mathrm{CO}(X\ ^1\Sigma^+) \rightarrow \mathrm{CO_2}(X\ ^1\Sigma_g^+) + \mathrm{C}(^3P/^1D). \quad (2)$$

As found in photochemical and theoretical studies of carbon monoxide, the $^1\Sigma^+$ ground state can be electronically excited by wavelengths as large as 1538 Å (8.07 eV) for the $A\ ^1\Pi \leftarrow X\ ^1\Sigma^+$ transition or 2055 Å (6.04 eV) for the spin forbidden $a\ ^3\Pi \leftarrow X\ ^1\Sigma^+$ transition (Cooper & Langhoff 1981; Cooper & Kirby 1987). The latter dissociation pathway requires much less energy than the traditional direct dissociation mechanism or a predissociation mechanism as reported by van Dishoeck (1987), which requires at least 11.1 eV (Reddy et al. 2003):

$$\mathrm{CO}(X\ ^1\Sigma^+) \rightarrow \mathrm{C}(^3P/^1D) + \mathrm{O}(^3P/^1D). \quad (3)$$

An important consequence of the dissociation via reaction (2) is that no oxygen atoms are produced during the irradiation, which should be an obvious effect when analyzing the products of the current experiment. Note that carbon dioxide was the only oxygen-rich molecule observed in the Gerakines et al. (1996) photolysis experiment, which supports this conclusion. The dissociation pathway of carbon monoxide by reaction (2) was subsequently supported by Gerakines & Moore (2001) and Cottin et al. (2003) in their photolysis experiments.

4.2. *The Reaction Model*

We have developed a model that shows the reaction pathways taken to form the products during the irradiation of the carbon monoxide ice (Fig. 10). Using this model, the kinetics and mechanisms for the formation of the various products can be understood. This reaction model assumes the dissociation pathway of carbon monoxide via reaction (2). The most important consequence of this, as opposed to the direct dissociation mechanism (eq. [3]) is that no free oxygen atoms should be in the ice to undergo reaction. Based on the observed products (Table 2), there is actually no evidence of oxygen reacting in the sample. Carbon dioxide was the only oxygen-rich molecule that was confirmed after irradiation to be formed via equation (2). As seen in previous experiments (Bennett et al. 2004; Gerakines & Moore 2001; Brucato et al. 1997), if ground state carbon dioxide molecules and free oxygen atoms were present, the cyclic, C_{2v} symmetric, carbon trioxide isomer should be readily observed:

$$\mathrm{CO_2}(X\ ^1\Sigma_g^+) + \mathrm{O}(^3P/^1D) \rightarrow \mathrm{CO_3}(X\ ^1A_1). \quad (4)$$

However, as Bennett et al. (2004) have pointed out, the oxygen atoms need to be either electronically excited or suprathermal (kinetically excited) to react. Otherwise, a barrier of approximately 145 kJ mol^{-1} exists that is insurmountable at the low temperatures of a cold molecular cloud and in this experiment. From the lack of detection of the cyclic carbon trioxide molecule, it is clear that electronically excited or suprathermal oxygen atoms are not produced during irradiation. This does not discount the presence of ground state oxygen atoms. However, the oxygen and ozone molecules, which were observed neither by mass spectrometry nor by FTIR spectroscopy, are produced by barrierless reactions of ground state oxygen atoms:

$$\mathrm{O}(^3P) + \mathrm{O}(^3P) \rightarrow \mathrm{O_2}(X\ ^3\Sigma_g^-), \quad (5)$$

$$\mathrm{O_2}(X\ ^3\Sigma_g^-) + \mathrm{O}(^3P) \rightarrow \mathrm{O_3}(X\ ^1A_1). \quad (6)$$

This is a similar reaction sequence as with carbon atoms to form the observed C_3 molecule (§ 4.6). If oxygen atoms were present

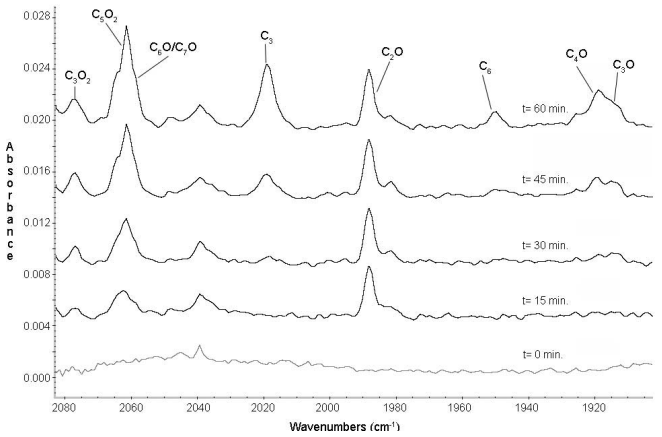

FIG. 11.—Infrared spectrum of the carbon monoxide ice is shown for different times of irradiation between 2080 and 1900 cm^{-1}. This demonstrates the temporal evolution of the column densities of the molecules, which are used in the following figures to understand the kinetics formation pathways.

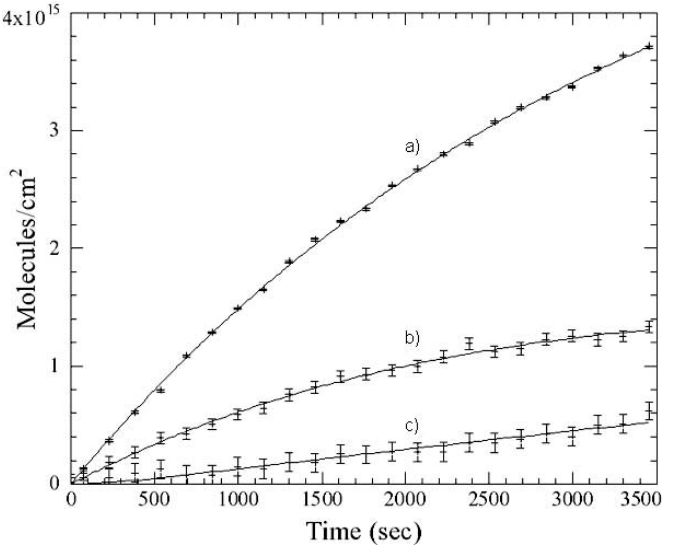

FIG. 12.—Plot of the temporal evolution of the column densities of (*a*) carbon dioxide (2346 cm^{-1} band), (*b*) carbon suboxide (2242 cm^{-1} band), and (*c*) tricarbon monoxide (1913 cm^{-1} band) was made and the kinetic equations derived from the reaction model were fitted to the data. Error bars are $\pm 4 \times 10^{12}$ molecules cm^{-2}, $\pm 5 \times 10^{13}$ molecules cm^{-2}, and $\pm 8 \times 10^{13}$ molecules cm^{-2}, respectively.

in the ice, ozone would also be expected to form, even if in only minor abundances. The nondetection of carbon trioxide, oxygen, and ozone is not evidence enough to state that no oxygen atoms are produced from the decomposition of carbon monoxide, but we can say that their abundance does not play a large role in the observed routes of reaction of the linear, carbon-bearing molecules in the ice sample. Consequently, it seems safe to say that the dissociation of carbon monoxide follows a reaction route as previously shown in equation (2) and that oxygen atoms do not play a role in the reaction pathways to the observed products. Therefore, oxygen atoms are not included in the reaction model (Fig. 10).

Using this reaction model, we can begin to understand the kinetics and mechanisms associated with the reaction pathways. Throughout the irradiation phase of the experiment, molecules were observed to arise at different times and at different rates (see Fig. 11). For example, the 1988 cm^{-1} peak of C_2O became observable and reached its equilibrium abundance almost immediately, whereas the assignment of C_6 at 1951 cm^{-1} was only detected after a long irradiation time. By plotting the column densities of each molecule versus irradiation time, the temporal evolution of the products can be identified. Note that the error bars associated with these data points were determined by integrating a featureless region of the infrared spectrum and then incorporating this noise level into the calculations for the column densities of each molecule. We can further fit the temporal evolutions with reaction rates. Hence, kinetic equations were derived according to the proposed reaction model (see Appendix B). Then all equations were simultaneously fitted to the experimentally observed temporal evolution plots of column densities of the observed molecules versus time in order to obtain rate constants for the different reaction pathways. In the following sections, each product will be investigated to understand how it forms by using data from the kinetic fits and published energetics values.

4.3. *Carbon Dioxide,* $CO_2(X\ ^1\Sigma_g^+)$

The carbon dioxide molecule in its $X\ ^1\Sigma_g^+$ electronic ground state is important in a great variety of interstellar and planetary environments. It has been observed in large abundances on interstellar ice grains, in comets, and in the ices of many planets and satellites in the solar system (Cruikshank et al. 1993; Guertler et al. 1996; Ehrenfreund et al. 1997a; Buratti et al. 2005). As seen in this experiment, carbon dioxide is produced from the irradiation of carbon monoxide at short times to yield a high column density of $(3.71 \pm 0.01) \times 10^{15}$ molecules cm^{-2} after 60 minutes of irradiation. As mentioned in the introduction, the presence of carbon dioxide on Triton could be explained by this sort of radiation processing of carbon monoxide ice. It is assumed that Triton has a similar initial chemical inventory to that of Pluto because they were thought to have formed at similar distances from the Sun; however, carbon dioxide has not been detected on Pluto. This could be due to a difference in history of the bodies rather than initial chemical abundances. The radiation environment of Pluto is much weaker with no magnetospheric ion or electron bombardment as on Triton, so the ice would not be processed to the same degree explaining the nondetection of carbon dioxide on Pluto.

A graph of the temporal evolution of the column density of carbon dioxide was fitted with a pseudo–first-order kinetic equation as seen in Figure 12. This assumes that the time it takes to electronically excite a carbon monoxide molecule (eq. [1]) is negligible and, hence, the rate constant is fast when compared to two carbon monoxide molecules reacting to form a carbon dioxide molecule plus a carbon atom (eq. [2]). The temporal dependence of the column density of carbon dioxide is then given by equation (7). The best-fit values were found to be $a = (5.8 \pm 0.1) \times 10^{15}$ molecules cm^{-2} and $k_1 = (2.96 \pm 0.07) \times 10^{-4}$ s^{-1} (Table 5):

$$[CO_2](t) = a(1 - e^{-k_1 t}). \quad (7)$$

Note that a pseudo–first-order fit was used to describe the temporal evolution of the carbon dioxide column density. This assumes that carbon dioxide is not destroyed or does not react onward once produced.

However, it must be recognized that free carbon atoms formed via equation (2) could subsequently react with carbon dioxide in the matrix. If carbon atoms are produced, they could add to one of the double bonds of carbon dioxide to produce the C_2O_2 molecule. Mechanistically speaking, since the carbon atom has empty *p*-orbitals, it can act much like a Lewis acid and accepts π-electrons from a double bond in the carbon dioxide molecule

TABLE 5
IMPORTANT REACTIONS IN THIS STUDY

Reactants	Products	Rate Constant, k (s^{-1})	Reaction Energy, $\Delta_R G$ (kJ mol^{-1})
CO* + CO ($X\,^1\Sigma^+$)	CO_2 ($X\,^1\Sigma_g^+$) + C ($^3P/^1D$)	$k_1 = (2.96 \pm 0.07)\text{E}{-4}$	...
CO_2($X\,^1\Sigma_g^+$) + C (^3P)	C_2O_2 ($X\,^3\Sigma_g^-$)	...	−287.5
C_2O_2 ($X\,^3\Sigma_g^-$)	2CO ($X\,^1\Sigma^+$)	...	−254.0
CO ($X\,^1\Sigma^+$) + C (^3P)	C_2O ($X\,^3\Sigma^-$)	$k_2 = (3.5 \pm 0.5)\text{E}{-3}$	−209.1
CO ($X\,^1\Sigma^+$) + C_2 ($X\,^1\Sigma_g^+$)	C_3O ($X\,^1\Sigma^+$)	...	−365.7
C (^3P) + C_2O ($X\,^3\Sigma^-$)	C_3O ($X\,^1\Sigma^+$)	$k_3 = (3.11 \pm 0.08)\text{E}{-6}$	−743.2
C (^3P) + C_3O ($X\,^1\Sigma^+$)	C_4O ($X\,^3\Sigma^-$)	$k_4 = (2.5 \pm 0.1)\text{E}{-5}$	−420.0
CO ($X\,^1\Sigma^+$) + C_3 ($X\,^1\Sigma_g^+$)	C_4O ($X\,^3\Sigma^-$)	...	−78.9
C_2 ($X\,^1\Sigma_g^+$) + C_3O ($X\,^1\Sigma^+$)	C_5O ($X\,^1\Sigma^+$)	...	−537.6
C (^3P) + C_4O ($X\,^3\Sigma^-$)	C_5O ($X\,^1\Sigma^+$)	$k_5 = (7.00 \pm 0.07)\text{E}{-4}$	−704.3
CO ($X\,^1\Sigma^+$) + C_2O ($X\,^3\Sigma^-$)	C_3O_2($X\,^1\Sigma_g^+$)	$k_6 = (4.0 \pm 0.4)\text{E}{-5}$	−346.4
C (^3P) + 2CO ($X\,^1\Sigma^+$)	C_3O_2($X\,^1\Sigma_g^+$)	$k_7 = (4 \pm 1)\text{E}{-5}$	−555.5
CO ($X\,^1\Sigma^+$) + C_3O ($X\,^1\Sigma^+$)	C_4O_2 ($X\,^3\Sigma_g^-$)	$k_{10} = 0$	−12.7
C (^3P) + C_3O_2($X\,^1\Sigma_g^+$)	C_4O_2 ($X\,^3\Sigma_g^-$)	$k_8 = (4.1 \pm 0.1)\text{E}{-4}$	−409.5
C (^3P) + C_4O_2 ($X\,^3\Sigma_g^-$)	C_5O_2($X\,^1\Sigma_g^+$)	$k_9 = (4.8 \pm 0.9)\text{E}{-8}$	−718.9
CO ($X\,^1\Sigma^+$) + C_4O ($X\,^3\Sigma^-$)	C_5O_2($X\,^1\Sigma_g^+$)	$k_{11} = (5.0 \pm 0.1)\text{E}{-4}$	−311.6
C_2O ($X\,^3\Sigma^-$) + C_3O ($X\,^1\Sigma^+$)	C_5O_2($X\,^1\Sigma_g^+$)	...	−522.4

NOTE.—The reactants and products are shown with their calculated rate constants, k, and reaction energies, $\Delta_R G$.

in a barrierless reaction. In a mechanism similar to that proposed for the formation of cyclic carbon trioxide (Bennett et al. 2004), the adding carbon atom would form a cyclic C_2O_2 intermediate. But unlike carbon trioxide, which is stabilized in this conformation, the cyclic C_2O_2 intermediate could ring open along a carbon-oxygen bond to yield the linear ethylenedione molecule, OCCO($X\,^3\Sigma_g^-$). Using the absolute energies calculated for carbon dioxide and for the ground state carbon atom (Table 6), the reaction toward the ethylenedione molecule is calculated to be exoergic by 287.5 kJ mol^{-1} (Table 5). However, the ethylenedione molecule has never been unequivocally observed in an experiment and is probably a very short-lived molecule that immediately dissociates to two carbon monoxide molecules:

$$\mathrm{CO_2}(X\ ^1\Sigma_g^+) + \mathrm{C}(^3P/^1D) \rightarrow \mathrm{C_2O_2}(X\ ^3\Sigma_g^-) \rightarrow 2\mathrm{CO}(X\ ^1\Sigma^+). \quad (8)$$

The ground state of the ethylenedione molecule ($X\,^3\Sigma_g^-$) is higher in energy than the two separated carbon monoxide

TABLE 6
TOTAL ENERGIES AND ZERO-POINT ENERGY CORRECTIONS OF VARIOUS SPECIES

	CCSD(T)/cc-pvqz			B3LYP/6-311G(d, p)		
MOLECULE	E_{total}	ZPE[a]	E_{total}+ZPE	E_{total}	ZPE	E_{total}+ZPE
C (^3P)	−37.786540	0.0	−37.786540	−37.855989	0.0	−37.855989
C (^1D)	−37.774442	0.0	−37.774442	−37.841028	0.0	−37.841028
C_2 ($X\,^1\Sigma_g^+$)	−75.800782	11.3	−75.796515	−75.900548	11.3	−75.896281
C_3 ($X\,^1\Sigma_g^+$)	−113.860464	21.3	−113.852264	−114.073963	21.3	−114.065763
C_4 ($X\,^3\Sigma_g^-$)	−151.827416	33.9	−151.814463	−152.128365	33.9	−152.115412
C_5 ($X\,^1\Sigma_g^+$)	−189.883772	50.2	−189.864599	−190.250594	50.2	−190.231421
C_6 ($X\,^3\Sigma_g^-$)	−227.859270	60.7	−227.836091	−228.313503	60.7	−228.290323
CO ($X\,^1\Sigma^+$)	−113.187862	13.4	−113.182805	−113.346235	13.4	−113.341178
C_2O ($X\,^3\Sigma^-$)	−151.057869	23.4	−151.048999	−151.301136	23.4	−151.292265
C_3O ($X\,^1\Sigma^+$)	−189.134143	40.6	−189.118617	−189.446630	40.6	−189.431105
C_4O ($X\,^3\Sigma^-$)	−227.084435	50.6	−227.065113	−227.484917	50.6	−227.465595
C_5O ($X\,^1\Sigma^+$)	−265.145481	66.9	−265.119915	−265.611954	66.9	−265.586388
C_6O ($X\,^3\Sigma^-$)	−303.114720	76.6	−303.085513	−303.668394	76.6	−303.639186
C_7O ($X\,^1\Sigma^+$)	−341.164532	95.8	−341.128023	−341.784178	95.8	−341.747669
CO_2 ($X\,^1\Sigma_g^+$)	−188.384545	31.0	−188.372824	−188.641139	31.0	−188.629418
C_2O_2 ($X\,^3\Sigma_g^-$)	−226.283263	37.7	−226.268876	−226.630464	37.7	−226.616077
C_3O_2 ($X\,^1\Sigma_g^+$)	−264.385717	57.7	−264.363745	−264.799747	57.7	−264.777776
C_4O_2 ($X\,^3\Sigma_g^-$)	−302.331355	65.7	−302.306261	−302.831611	65.7	−302.806518
C_5O_2 ($X\,^1\Sigma_g^+$)	−340.397795	82.0	−340.366604	−340.965394	82.0	−340.934203
C_6O_2 ($X\,^3\Sigma_g^-$)	−378.364047	92.9	−378.328618	−379.017329	92.9	−378.981900

NOTES.—Total energies (atomic units, 1 a.u. = 2625.50 kJ mol^{-1}) and zero-point energy corrections ZPE (kJ mol^{-1}) of various species calculated at the CCSD(T)/cc-pvqz and the B3LYP/6-311G(d, p) levels of theory. The CCSD(T)/cc-pvqz values were used to calculate the energies of reactions presented in this paper.

[a] Calculated at the B3LYP/6-311G(d, p) level.

molecules. Our calculations show the energy to be strongly exoergic by 254.0 kJ mol^{-1}, while Talbi & Chandler (2000) calculated the difference to be 245.0 kJ mol^{-1}. Therefore, dissociation of ethylenedione from its ground state is dependent on whether there exists an efficient curve crossing from the triplet to the singlet surface and whether the barrier can be passed. This has been calculated to be the case by Schröder et al. (1998), where the conical intersection point lies 13 kJ mol^{-1} above the triplet ground state of ethylenedione. The reaction sequence in equation (8) would show an efficient means of regenerating the carbon monoxide molecule from carbon dioxide. However, the current experimental setup cannot elucidate whether equation (8) is an important reaction pathway to destroy carbon dioxide. If it were, the carbon dioxide column density would need to be fitted with an A←B←C type consecutive reaction where carbon dioxide would be at position B, rather than a pseudo–first-order reaction (A←B) as reported. Future studies are planned using isotopically labeled carbon monoxide to understand whether the carbon dioxide plus carbon atom reaction plays a significant role in this experiment.

Previously, there have been kinetic studies that investigated the reaction between ground state carbon atoms, generated by flash photolysis of carbon suboxide, and carbon dioxide at 300 K (Husain & Kirsch 1971; Husain & Young 1975). However, with the high temperature and the low collision frequency of these experiments, the ethylenedione intermediate was not stabilized and immediately dissociated to two carbon monoxide molecules. An upper limit of the rate constant for this gas phase reaction was derived from these experiments to be 1.0×10^{-14} cm^3 molecules^{-1} s^{-1}. This shows that the carbon dioxide plus carbon atom reaction could occur, but it is still unclear that this pathway is important in our low-temperature, solid state system.

4.4. C_nO *Molecular Species*

Although only C_2O and C_3O have been detected in interstellar space, the higher order members of the C_nO series are also thought to have significant abundances (Adams et al. 1989). These molecules are linear in geometry with cummulene-like bonding, and their electronic structure alternates between closed-shell ($X\,^1\Sigma^+$) for C_nO, n = odd, and open-shell ($X\,^3\Sigma^-$) for C_nO, n = even. This means that the species with an odd number of carbon atoms will be more stable and, hence, less reactive than their even numbered counterparts. Note that all C_nO molecules ($n \leq 9$) have been shown to have negative enthalpies of formation (Moazzen-Ahmadi & Zerbetto 1995).

4.4.1. *Dicarbon Monoxide,* $C_2O(X\,^3\Sigma^-)$

The ketenylidene molecule, CCO($X\,^3\Sigma^-$), was first detected in the gas phase of the cold molecular cloud TMC-1 (Ohishi et al. 1991), although it was found to have a low fractional abundance relative to H_2 of only about 6×10^{-11}. As the first member in the C_nO series of molecules beyond the abundant carbon monoxide molecule, understanding its production is important to identify the reaction processes that form the higher order species. Ohishi et al. (1991) reviewed probable formation processes of ketenylidene via ion-molecule reactions in the gas phase. However, in the solid state in our experiments, there has been no evidence of ions being produced and, so, the production of C_2O must follow a different mechanism. As carbon atoms are produced by irradiation, they can react with the carbon monoxide molecules in the ice. There are two probable routes of reaction. First, the carbon atoms can add to the nonbonding electrons on the carbon of the carbon monoxide molecule. The second option is for the carbon atom to add to the carbon-oxygen triple bond to possibly form a cyclic intermediate structure, which would subsequently ring open along a C-O bond to give the linear CCO($X\,^3\Sigma^-$) molecule. This pathway would have a larger cone of acceptance and, hence, an enhanced reactive cross section. Neither route should have a barrier to the initial carbon addition (Kaiser 2002):

$$\mathrm{CO}(X\,^1\Sigma^+) + \mathrm{C}(^3P/^1D) \xrightarrow{k_2} \mathrm{C_2O}(X\,^3\Sigma^-). \quad (9)$$

Zengin et al. (1996) calculated this reaction, using C(^3P), to be exothermic by 220 ± 20 kJ mol^{-1} using theoretically derived thermodynamic values, while our ab initio calculations give an exoergicity of 209.1 kJ mol^{-1}. Plotting the evolution of the column density of dicarbon monoxide through time, the abundance is seen to reach equilibrium within 10 minutes of radiation time and then remain essentially constant (see Fig. 13). A kinetic equation was obtained (see Appendix B) that takes into account the formation of C_2O (k_2) as well as its destruction to C_3O (k_3) and C_3O_2 (k_6) as laid out in the reaction model (Fig. 10). While the values of k_3 and k_6 will be reported as they pertain to the formation of their respective molecules, k_2 was calculated to be $(3.5 \pm 0.5) \times 10^{-3}$ s^{-1}. The ketenylidene molecule has a high formation rate because of the barrierless and exoergic routes of formation between reactants of high abundances. However, the column density at the end of irradiation is only $(9.2 \pm 0.5) \times 10^{13}$ molecules cm^{-2}. This is a very low abundance for a molecule formed this early in the reaction sequence but can be explained by a high rate of destruction as would be expected with open-shell triplet species. Also, it is shown later that it is energetically very favorable for C_2O to react onward to C_3O or C_3O_2 (§§ 4.4.2 and 4.5.1).

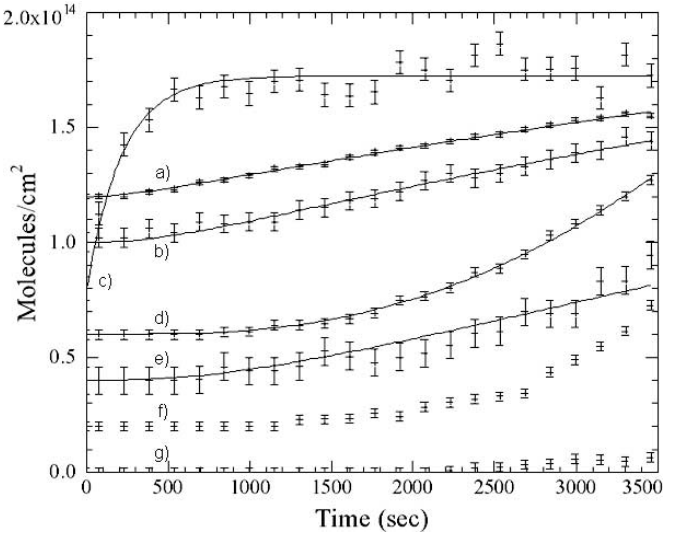

FIG. 13.—Plot of the temporal evolution of the column densities of (*a*) C_4O_2 (2122 cm^{-1} band), (*b*) C_5O_2 (2059 cm^{-1} band), (*c*) dicarbon monoxide (1988 cm^{-1} band), (*d*) C_5O (2106 cm^{-1} band), (*e*) C_4O (1919 cm^{-1} band), (*f*) C_3 (2019 cm^{-1} band), and (*g*) C_6 (1951 cm^{-1} band) was made. For all except C_3 and C_6, the derived kinetic equations from the reaction model were fitted to the data. The profiles have been each offset by 2×10^{13} molecules cm^{-2} to maintain clarity of the data. Error bars are (*a*) $\pm 1 \times 10^{12}$ molecules cm^{-2}, (*b*) $\pm 4 \times 10^{12}$ molecules cm^{-2}, (*c*) $\pm 5 \times 10^{12}$ molecules cm^{-2}, (*d*) $\pm 2 \times 10^{12}$ molecules cm^{-2}, (*e*) $\pm 6 \times 10^{12}$ molecules cm^{-2}, (*f*) $\pm 2 \times 10^{12}$ molecules cm^{-2}, and (*g*) $\pm 2 \times 10^{12}$ molecules cm^{-2}.

4.4.2. *Tricarbon Monoxide,* $C_3O(X\,^1\Sigma^+)$

Tricarbon monoxide was the first linear carbon-chain molecule containing oxygen that was observed in space. It was detected by Matthews et al. (1984) in the gas phase of the Taurus Molecular Cloud (TMC-1) using radio astronomy. Gas phase synthesis reactions forming C_3O have been investigated by

Herbst et al. (1984) and by Brown et al. (1985b) using ion-molecule, dissociative recombination, and neutral-neutral reactions. In the solid state there exist two different pathways to the formation of C_3O. A dicarbon molecule $C_2(X\ ^1\Sigma_g^+)$ can react with a carbon monoxide molecule $CO(X\ ^1\Sigma^+)$ at either the nonbonding electron pair of the carbon of the carbon monoxide or via addition to the carbon-oxygen triple bond followed by isomerization steps and ring opening:

$$CO(X\ ^1\Sigma^+) + C_2(X\ ^1\Sigma_g^+) \rightarrow C_3O(X\ ^1\Sigma^+). \quad (10)$$

Maclagan & Sudkeaw (1993) calculated the C_3O molecule to lie 453.1 kJ mol^{-1} below the ground state reactants, where our calculations show the C_3O molecule to be 365.7 kJ mol^{-1} below the separated reactants. They found that the reverse reaction is the lowest energy dissociation pathway of tricarbon monoxide. However, the dicarbon molecule was not observed in our experiment, making it impossible at present to report the kinetics of this pathway.

A second possible pathway is the reaction of a ketenylidene molecule with a carbon atom via

$$C_2O(X\ ^3\Sigma^-) + C(^3P/^1D) \rightarrow C_3O(X\ ^1\Sigma^+). \quad (11)$$

Here the carbon atom can add to the nonbonding electron pair of the carbon atom of the dicarbon monoxide molecule, or across the double bond of the dicarbon monoxide molecule followed by ring opening to form tricarbon monoxide, similar to the formation of dicarbon monoxide. If reaction proceeds with an electronically excited carbon atom (^1D), intersystem crossing would need to occur to form the product on the ground state singlet surface. Assuming ground state electronic configurations, this reaction is exoergic by 743.2 kJ mol^{-1} (691.7 kJ mol^{-1} as calculated from values in Maclagan & Sudkeaw 1993). Comparing the energies of formation of C_3O with the energy of formation of C_2O, the tricarbon monoxide molecule is energetically favored, existing as a closed-shell singlet species, whereas dicarbon monoxide is an open-shell triplet species. This is to say that once C_2O is formed, it should easily react onward to C_3O provided there are available carbon atoms in the matrix. The rate constant (k_3) associated with the reaction in equation (11) was found to be $(3.11 \pm 0.08) \times 10^{-6}$ s^{-1} after finding the best fit to the temporal development of the C_3O column density (Fig. 12). Comparing column densities after 60 minutes of irradiation, the tricarbon monoxide abundance is enhanced by nearly 7 times that of dicarbon monoxide. Ohishi et al. (1991) found this value to be about two along a line of sight in TMC-1 in the gas phase.

4.4.3. $C_4O(X\ ^3\Sigma^-)$

The C_4O molecule has not been observed in interstellar space, but evident by its abundance of only 2 times less than C_2O at the end of the irradiation phase of our experiment, a detectable amount is likely in TMC-1, where many other carbon-chain molecules have been observed. In accordance with the reaction model, the kinetics of the formation of C_4O via a reaction between tricarbon monoxide and a carbon atom was investigated. As in the formation of C_2O and C_3O, a free carbon atom can either react at the nonbonding electron pair of the carbon atom or add across one of the double bonds of the C_3O molecule followed by ring opening. The rate of formation of C_4O gives insight to which mechanism predominates. Fitting the derived rate equation to the column density of C_4O plotted over time (Fig. 13), the rate of formation (k_4) was found to be $(2.5 \pm 0.1) \times 10^{-5}$ s^{-1}. This value is greater than the rate of formation of C_3O (k_3) by an order of magnitude. This is unexpected, since the tricarbon monoxide molecule is energetically more stable relative to its precursors than the C_4O molecule. Our calculations show that the formation of C_4O by ground state reactants in equation (12) is exoergic by 420.0 kJ mol^{-1}:

$$C_3O(X\ ^1\Sigma^+) + C(^3P/^1D) \xrightarrow{k_4} C_4O(X\ ^3\Sigma^-). \quad (12)$$

The C_4O molecule also has a relatively low energy dissociation pathway of 78.9 kJ mol^{-1} to $C_3(X\ ^1\Sigma_g^+)$ and $CO(X\ ^1\Sigma^+)$, assuming C_4O can undergo intersystem crossing to dissociate on the singlet surface (42.3 kJ mol^{-1}, as calculated by Ewing 1989). The fact that the rate of formation of C_4O is faster than that for C_3O, while not being consistent with energetics considerations, means that the justification must lie in the mechanism. The discrepancy can be rationalized if the major route of formation of the C_nO species is by a carbon atom adding across a double bond of the $C_{n-1}O$ molecule followed by a rearrangement or ring opening. A carbon atom adding to C_3O to form C_4O (eq. [12]) has a greater possible area of reaction because of the extra double bond than it does when reacting with C_2O to form C_3O (eq. [11]), i.e., the cone of acceptance of the C_3O molecule is larger than the one from the C_2O molecule. This translates to a higher rate of reaction. This mechanism would also be predicted to dominate over reaction at the nonbonding electron pair on the terminal carbon atom based on the greater cone of acceptance of π-bonds. Using this logic, it would be assumed that the rate of formation of C_5O (k_5) would be even greater than for C_4O. This is in fact what is found.

4.4.4. $C_5O(X\ ^1\Sigma^+)$

With an odd number of carbon atoms, the C_5O molecule is a closed-shell molecule that is relatively stable to dissociation. Botschwina et al. (1995) carried out a theoretical investigation of the molecule and found the lowest energy, spin-allowed dissociation channel (eq. [13]) to have an energy of 532 kJ mol^{-1} after zero-point correction, which closely agrees with the theoretical value found from our calculations of 537.6 kJ mol^{-1}:

$$C_5O(X\ ^1\Sigma^+) \rightarrow C_3O(X\ ^1\Sigma^+) + C_2(X\ ^1\Sigma_g^+). \quad (13)$$

As previously mentioned, the predominant formation route of C_5O probably is the addition of a carbon atom to one of the double bonds of the C_4O molecule, which then rearranges or ring opens to the linear C_5O structure:

$$C_4O(X\ ^3\Sigma^-) + C(^3P/^1D) \xrightarrow{k_5} C_5O(X\ ^1\Sigma^+). \quad (14)$$

This reaction is calculated to be exoergic by 704.3 kJ mol^{-1}. After fitting the kinetic equation derived for the C_5O molecule to the column density plot (Fig. 13), the rate of formation was best fitted to $k_5 = (7.00 \pm 0.07) \times 10^{-4}$ s^{-1}. The C_4O molecule has a larger cone of acceptance where a carbon atom can attack (compared to C_2O and C_3O); therefore, the formation of C_5O can proceed at a higher rate than for the formation of C_3O or C_4O. A comparison with the formation of C_2O has been left out of this discussion because a carbon atom reacting with the double bond of a carbon monoxide molecule should be much faster compared to a carbon atom attacking a cummulene structure (Kaiser 2002). Carbon monoxide has a high availability of reactive electron density around the carbon atom, so there are fewer geometrical considerations that an attacking carbon atom must consider. This is because the carbon monoxide molecule has a triple bond; thus, the electron density of the π-orbitals extend around the entire molecule, allowing for a greater area where an attacking carbon

atom can react. On the other hand, a carbon atom reacting with a cummulene molecule with a double bond has roughly half of the possible area to react per bond (only one π bond). In cummulenes, π-bonds alternate; two adjacent π-bonds are always located in perpendicular planes, so it is more than one π-bond, but, of course, spatial requirements for the attacking carbon are more stringent than in the case of CO, where atomic carbon can attack both the π bonds. Once a carbon atom is produced during irradiation, there should immediately be a CO molecule in the correct orientation for reaction in the matrix, whereas with a higher order carbon oxide, the correct reaction geometry of the reactants is crucial. This is reflected by the very fast rate constant, k_2, to form dicarbon monoxide (§ 4.4.1). The next two reactions in the sequence of the formation of the C_nO species would be to form $C_6O(X\,^3\Sigma^-)$ and then $C_7O(X\,^1\Sigma^+)$. However, as mentioned in § 3.1, assigning these molecules to the observed absorptions is ambiguous. Therefore, an investigation of the kinetics of these molecules was omitted in this discussion.

4.5. C_nO_2 *Molecular Species*

The oxycummulenes are very interesting astrochemical molecules. Their ground state electronic configurations are similar to the C_nO molecules, where an odd number of carbons give a singlet state ($X\,^1\Sigma_g^+$), while an even number of carbons give the triplet state ($X\,^3\Sigma_g^-$). The simplest oxycummulene, carbon dioxide (§ 4.3), is very stable and abundant in the interstellar medium. Even though higher order C_nO_2 molecules are also expected to be stable and moderately abundant in the ISM, their symmetry prohibits gas phase detection via radio (rotational) spectroscopy, and there may not be sufficient amounts on grains to be observed in the solid state using infrared spectroscopy. However, as seen in § 4.8, grains that have been thermally processed may have an increased abundance of oxycummulenes relative to the host ice on the grain due to their low vapor pressure at these temperatures so that their detection would be more probable.

4.5.1. *Carbon Suboxide,* $C_3O_2(X\,^1\Sigma_g^+)$

This molecule has been the subject of numerous investigations because of its suspected relevance to interstellar ices and comets. It has been intensely experimentally studied in the solid state using infrared spectroscopy—for example, Miller & Fateley (1964) and Hayden Smith & Leroi (1966) to name a few. More recently, carbon suboxide has been studied as a product of irradiated carbon monoxide ice (Gerakines & Moore 2001; Trottier & Brooks 2004). Although C_3O_2 has not been observed in any extraterrestrial environments, its ease of production seen in these experiments indicates that carbon suboxide should be a relatively abundant interstellar molecule when high abundances of solid carbon monoxide are present. According to our reaction model, carbon suboxide would be produced by the highly reactive dicarbon monoxide molecule ($X^3\Sigma^-$) bonding with a carbon monoxide molecule ($X\,^1\Sigma^+$) in the ice matrix, accompanied by intersystem crossing:

$$C_2O(X\ ^3\Sigma^-) + CO(X\ ^1\Sigma^+) \xrightarrow{k_6} C_3O_2(X\ ^1\Sigma_g^+). \quad (15)$$

Using energetics from Table 6, this reaction was calculated to be exoergic by 346.4 kJ mol^{-1}. Fitting the temporal evolution of the column density of C_3O_2 (Fig. 12) to the derived kinetic equation from the reaction model, the rate constant for this route of reaction, k_6, was found to be $(4.0 \pm 0.4) \times 10^{-5}$ s^{-1}. However, this pathway, through the dicarbon monoxide intermediate, could not alone account for the observed abundance of carbon suboxide. Therefore, an additional pathway was added, as seen in the reaction model, in which a carbon atom will simultaneously react with two carbon monoxide molecules in a concerted reaction to form carbon suboxide:

$$C(^3P/^1D) + 2CO(X\ ^1\Sigma^+) \xrightarrow{k_7} C_3O_2(X\ ^1\Sigma_g^+). \quad (16)$$

This pathway is energetically favorable by 555.5 kJ mol^{-1}, where the rate constant, k_7, was found to be $(4 \pm 1) \times 10^{-5}$ s^{-1}.

4.5.2. $C_4O_2(X\ ^3\Sigma_g^-)$

With the alteration between singlet and triplet electronic ground states for different number of carbon atoms of the oxycummulene molecules, the C_4O_2 molecule is found to be an open-shell species, existing on the triplet surface. As shown in the reaction model, there exist two primary routes of formation. The first pathway entails a reaction between tricarbon monoxide and carbon monoxide and would require intersystem crossing:

$$C_3O(X\ ^1\Sigma^+) + CO(X\ ^1\Sigma^+) \xrightarrow{k_{10}} C_4O_2(X\ ^3\Sigma_g^-). \quad (17)$$

However, the reactants are two closed-shell, singlet species, which should have a barrier to react with each other. Also, the reactants exist only slightly higher than the product (12.7 kJ mol^{-1}). These arguments seem to say that the pathway presented in equation (17) should not be a major formation pathway to C_4O_2 at 10 K. In fact, this is what is calculated by simultaneously fitting the kinetic equations to the column densities of the molecular species in the reaction model. The rate constant, k_{10}, was found to be zero, indicating that this pathway does not exist. The most probable mechanism for the formation of C_4O_2 is then the addition of a carbon atom to a double bond on the carbon suboxide molecule to from a cyclic intermediate that can ring open to the linear C_4O_2 structure:

$$C_3O_2(X\ ^1\Sigma_g^+) + C(^3P/^1D) \xrightarrow{k_8} C_4O_2(X\ ^3\Sigma_g^-). \quad (18)$$

This reaction is calculated to be exoergic by 409.5 kJ mol^{-1} and has a rate constant, k_8, of $(4.1 \pm 0.1) \times 10^{-4}$ s^{-1} when fitted to the temporal evolution of the column density of C_4O_2 (Fig. 13). A final possible pathway entails the reaction of two dicarbon monoxide molecules bonding to each other at their terminal carbon atoms followed by an intersystem crossing to the triplet surface. However, this pathway was not included in the model, and it is unclear if the C_2O molecule builds up enough abundance to have a high probability of reacting with another C_2O molecule to form C_4O_2 before reacting with CO or a carbon atom.

4.5.3. $C_5O_2(X\ ^1\Sigma_g^+)$

The C_5O_2 molecule is the longest carbon-chain oxycummulene that has been experimentally observed. It is a valid, astrophysically relevant molecule with its closed-shell ground electronic state. While there are many possible routes of formation for the C_5O_2 molecule, two were investigated in this study. First, a carbon atom can add to one of the double bonds of the C_4O_2 molecule to form C_5O_2 in a mechanism similar to that from equation (18):

$$C_4O_2(X\ ^1\Sigma_g^-) + C(^3P/^1D) \xrightarrow{k_9} C_5O_2(X\ ^1\Sigma_g^+). \quad (19)$$

This pathway is calculated to be energetically very favorable with an exoergicity of 718.9 kJ mol^{-1}; however, when the kinetics fits were made to the column density over time for C_5O_2

(Fig. 13), the rate constant, k_9, was calculated to be very small with a value of $(4.8 \pm 0.9) \times 10^{-8}$ s^{-1}. Investigating the other pathway of the stepwise reaction sequence, we see that the open-shell C_4O molecule could react with a carbon monoxide molecule to form C_5O_2:

$$C_4O(X\ ^3\Sigma^-) + CO(X\ ^1\Sigma^+) \xrightarrow{k_{11}} C_5O_2(X\ ^1\Sigma_g^+). \quad (20)$$

The rate constant according to this pathway, k_{11}, was fitted to be $(5.0 \pm 0.1) \times 10^{-4}$ s^{-1}, where the energy of this reaction was calculated to be exoergic by 311.6 kJ mol^{-1}. However, it must be remembered, especially with higher order products like C_5O_2, that there most likely exist other reaction pathways to the observed products. A stepwise synthesis has been assumed for the formation of the molecules observed in this experiment, which should be kinetically accurate for simple molecules, but the formation of higher order products may also readily occur via recombination of lower order products. For example, C_5O_2 could be produced in a reaction of C_2O and C_3O, which is energetically favorable by 522.4 kJ mol^{-1}. This is a limit in the current reaction model but due to the complexity and number of various routes of reaction, we cannot account for these pathways at present.

4.6. C_n *Species*

Only two pure carbon-chain molecules were observed in this experiment. They are the linear tricarbon molecule (2019 cm^{-1}) and the linear C_6 molecule (1951 cm^{-1}). The C_3 molecule has a long history of investigation (Weltner et al. 1964). It has been observed in interstellar space (Maier et al. 2001), comets (Rosen & Swings 1953; Rousselot et al. 2001), and toward cool carbon stars (McKellar 1948; Oka et al. 2003), and it is also an important product in flames (Ramsay 1959). Its formation route is seen in the reaction model, where a sequential process of carbon reactions would give tricarbon. According to a theoretical study by Raghavachari & Binkley (1987), reaction energies for the process $C + C_{n-1} \leftarrow C_n$ ($n = 2-10$) are all exoergic. This means once carbon atoms are formed they should quickly react to C_3 and without an energy barrier. But since the abundances of dicarbon and the carbon atom are impossible to trace with the current experimental setup, a kinetics analysis of the column density plot of tricarbon (Fig. 13) would have little meaning. However, due to the delayed increase of the column density of tricarbon, it is apparent that the C_3 molecule is formed as a higher order product, which agrees with the two-step synthesis seen in the reaction model. Similarly, C_6 is an energetically favorable molecule to produce, according to Raghavachari & Binkley (1987). The extremely late development of the 1951 cm^{-1} band (Fig. 13) indicates that the formation of C_6 indeed proceeds by a multistep reaction sequence as laid out in the reaction model. There are of course other formation routes—for example, the two closed-shell C_3 molecules bonding end on to form the linear C_6 molecule, or an open-shell reaction between a C_2 molecule and a C_4 molecule, both of which are energetically advantageous for stability considerations. The fact that there are a number of possible reaction pathways to C_6, along with the nondetection of C, C_2, C_4, and C_5, makes quantitative understanding the kinetics of the formation pathways to C_6 impossible at this stage.

4.7. *Postirradiation Isothermal Phase*

After the sample was irradiated for 60 minutes time, it was then kept at 10 K for another 60 minutes to check the stability of the molecules. Most species maintained a constant column density throughout this isothermal phase. However, the dicarbon monoxide molecule was found to be unstable under these conditions (Fig. 14). The column density spontaneously decreased according to two possible routes of destruction. The first would be the lowest energy direct dissociation channel to a carbon atom and a carbon monoxide molecule. As shown in the energetics analysis of C_2O, this would take at least 209.1 kJ mol^{-1}, energy that is unavailable in an unirradiated, thermally equilibrated ice at 10 K. The other possibility is for the dicarbon monoxide molecule to react with a matrix carbon monoxide molecule to form carbon suboxide in a barrierless reaction that is exoergic by 346.4 kJ mol^{-1} (eq. [15], § 4.5.1). This pathway is supported by a coincident increase in the column density of carbon suboxide during the isothermal phase (Fig. 14). These values are quantified to $(9.3 \pm 0.5) \times 10^{13}$ molecules cm^{-2} of C_2O being destroyed compared to $(2.8 \pm 0.7) \times 10^{14}$ molecules cm^{-2} of C_3O_2 produced. These values are not equivalent, being only slightly outside of their error limits, but this still supports the importance of this pathway in the reaction model. The C_4O molecule was also observed to decrease slightly during the steady state phase by $(7.4 \pm 0.8) \times 10^{13}$ molecules cm^{-2} or about 14% of its total abundance. The destruction mechanism is most likely the same as for the other open-shell triplet carbon oxide molecule, C_2O, but an increase in C_5O_2 abundance could not be observed due to other bands obscuring the absorption feature. Therefore, we can conclude that the reaction of the open-shell C_2O and C_4O species with carbon monoxide has no entrance barrier.

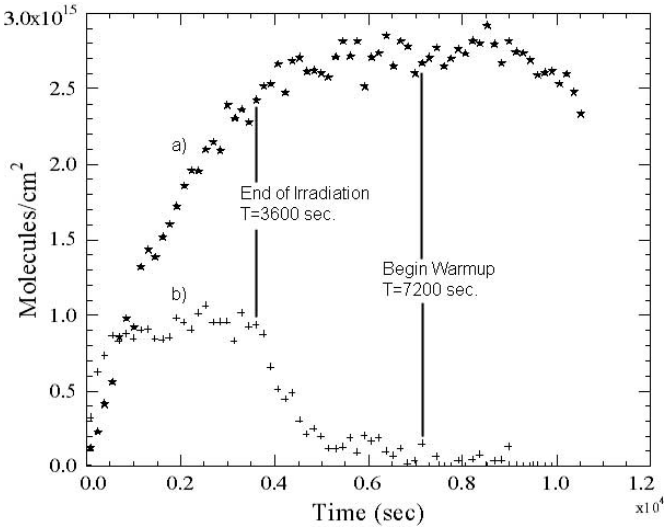

FIG. 14.—Temporal evolution of the column densities of (*a*) carbon suboxide and (*b*) dicarbon monoxide are plotted over the lifetime of C_2O. At the end of irradiation (3600 s.), the column density of C_2O began to decline until it had reached essentially zero by the time the warm-up phase had begun (7200 s.), whereas the carbon suboxide column density concurrently increased during this time. The dicarbon monoxide column density has been multiplied by a factor of 10 for a better comparison with the increase in the C_3O_2 column density.

4.8. *Warm-up Phase*

Following the 10 K isothermal phase in the absence of irradiation, the ice sample was warmed at a rate of 0.5 K minute^{-1}. When the sample had reached 17 K (8000 s on the experimental clock, where $t = 0$ s is the start of irradiation) the abundances of several molecular species began to change. As shown in Figure 15, the column density of tricarbon monoxide slowly decreased until around 31 K ($t = 9700$ s) when the carbon monoxide matrix started to sublime. In this temperature range, the

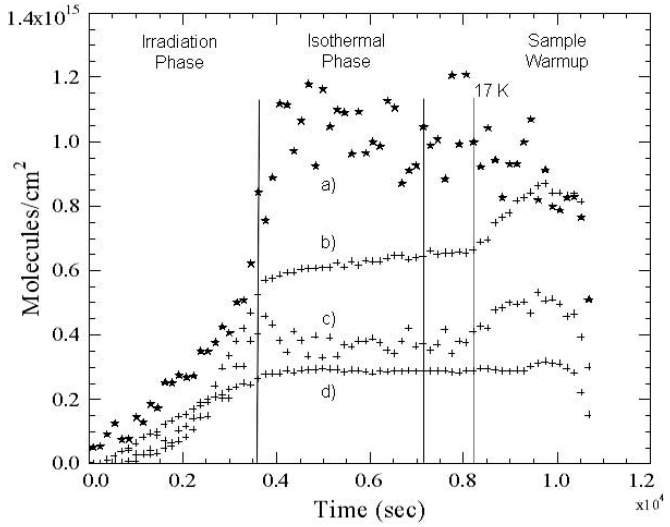

FIG. 15.—Temporal evolution of the column densities of (*a*) tricarbon monoxide, (*b*) C_5O, (*c*) C_4O, and (*d*) C_4O_2 are plotted until the carbon monoxide matrix sublimed at 40 K. The data represent abundances during the irradiation phase ($t = 0-3600$ s.), isothermal phase ($t = 3600-7200$ s.), and the warm-up phase ($t = 7200-10,800$ s.) of the experiment. The column densities for C_5O, C_4O, and C_4O_2 were multiplied by a factor of 7 to scale to the C_3O profile.

C_3O abundance decreased by $(3 \pm 1) \times 10^{14}$ molecules cm^{-2}. This coincided with an increase in the column densities of C_4O and C_5O (Fig. 15) until the matrix sublimed above 31 K. Their abundances increased by $(1.9 \pm 0.8) \times 10^{13}$ molecules cm^{-2} and $(3.1 \pm 0.6) \times 10^{13}$ molecules cm^{-2}, respectively. The decrease of C_3O could be explained by reaction with carbon atoms, which become mobile at these higher temperatures to form C_4O and then C_5O. More evidence of reaction with carbon atoms is seen by a small increase of the C_4O_2 column density [$(4 \pm 1) \times 10^{12}$ molecules cm^{-2}] in the same temperature range (Fig. 15). This increase could be due to carbon atoms reacting with the abundant carbon suboxide molecule as in equation (18). Unfortunately, a decrease in the carbon suboxide column density could not be confirmed because the amount destroyed would be within the error limits. However, it does seem that the carbon atom becomes mobile around 17 K and is observed to undergo barrierless reactions to form C_4O, C_5O, and C_4O_2.

As the sample was heated, the carbon monoxide ice matrix began to sublime at around 31 K. By 42 K, carbon monoxide and most of the other products from irradiation had either sublimed or reacted to thermally stable species. This is seen in Figure 16, where the only observable molecules remaining in the infrared spectrum at 42 K are CO_2, C_3O_2, and C_5O_2. The sublimation of carbon monoxide was confirmed by the quadrupole mass spectrometer (§ 3.3) that detected CO in the gas phase from 26 until 42 K. By 100 K the infrared spectrum indicated no carbon dioxide remaining in the ice sample to leave only C_3O_2 and C_5O_2 (Fig. 17). At this point another C_5O_2absorption band was identified at 2211 cm^{-1}. This agrees with the matrix isolation value Maier et al. (1988) found of 2213 cm^{-1} for the ν_2 vibration. In the analysis of the mass spectrometer data, carbon dioxide was observed to sublime primarily at 81 K, but the CO_2 signal did not completely diminish until above 100 K. As mentioned earlier, thermally processed interstellar dust grains may be enriched in oxycummulene molecules relative to the host ice on the grain. This is seen in our experiment, where the ice is chemically processed by radiation and then warmed to drive off the more volatile species, like carbon monoxide. The carbon suboxide was stable

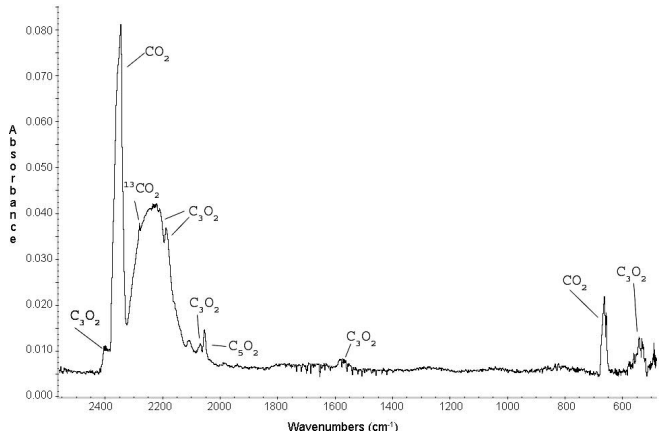

FIG. 16.—Infrared spectrum is shown from 2500 to 500 cm^{-1} at 40 K during warm-up, after the carbon monoxide ice had sublimed. The only remaining molecules observed on the substrate were carbon dioxide, carbon suboxide, and C_5O_2.

until about 100 K when it was detected in the gas phase by the mass spectrometer and until 125 K when the signal diminished (Fig. 8). This sublimation range is in agreement with Gerakines & Moore (2001), who reported a temperature of 120 K.

4.9. *Comparison with Previous Mechanistic Studies*

To our knowledge, there has been only one study that attempts to unravel the mechanisms for the production of higher order molecules resulting from irradiation of a carbon monoxide ice sample. Trottier & Brooks (2004) used 2 MeV protons to irradiate a carbon monoxide ice at 5 K; they also followed the products by infrared spectroscopy. These authors observed a series of products including CO_2, C_2O, and C_3O_2 as previously identified but also O_3, C_4O, C_5O_2, C_7O_2, and tentatively C_6. The presence of these newly identified molecules is surprising if stepwise mechanisms are assumed and the intermediate products are stable. For example, one would expect C_3O to be observed before the identification of C_4O (see above). Another interesting point is the production of ozone without carbon trioxide. If oxygen atoms were present in the ice, with enough abundance to form ozone, it seems that carbon trioxide should readily form as well, as seen by Bennett et al. (2004) in carbon dioxide irradiation

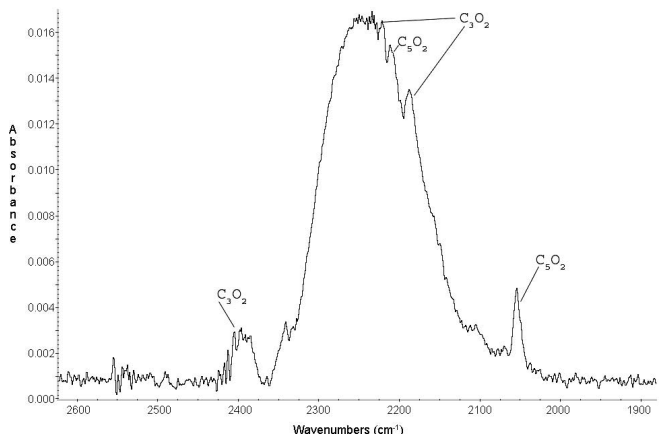

FIG. 17.—Infrared spectrum is shown from 2600 to 1900 cm^{-1} at 100 K during warm-up, after carbon monoxide and carbon dioxide had sublimed. The only remaining molecules observed on the substrate were carbon suboxide and C_5O_2.

experiments. Comparing our observed species with those seen by Trottier & Brooks (2004), there are a few noted differences. First, the peak that they had assigned to C_4O centered at 1919 cm^{-1} was found in our experiment to be made up of two overlapping absorptions. One is the C_4O peak at 1919 cm^{-1} and the other is at 1913 cm^{-1}, which we attribute to C_3O. Since the C_3O molecule precedes C_4O in a stepwise reaction sequence, its detection is expected before the C_4O molecule, especially when considering the greater stability of C_3O as reported in § 4.4.3. The other important difference between the Trottier & Brooks experiment when compared with the current work is that the 2106 cm^{-1} feature that was identified as the ozone molecule has been reassigned to C_5O. Due to the limited range of the spectrometer used in the aforementioned experiment (4000–1900 cm^{-1}), the most intense absorption of the ozone molecule at 1040 cm^{-1} was outside of their spectral window. The 1040 cm^{-1} peak is at least 10 times more intense than the 2106 cm^{-1} peak (Dyer et al. 1997); so our nondetection of the most intense absorption seems to preclude the presence of a detectable amount of ozone. The C_5O molecule was further confirmed with detection of its ν_3 vibrational mode at 1817 cm^{-1}, as previously discussed. A few other reassignments were also made, for example attributing C_4O_2 as the responsible molecule for the 2122 cm^{-1} absorption feature rather than C_7O_2, and the assignment of the 2019 cm^{-1} peak to C_3.

5. ASTROPHYSICAL IMPLICATIONS

Solid state carbon monoxide is found in a variety of low-temperature extraterrestrial environments. As seen in the present experiment, carbon monoxide had completely sublimed by 40 K, and so, the surfaces of Pluto (40 K) and Triton (38 K) mark the upper temperature limit to where carbon monoxide ice should be observed in the solid state. However, as comets intrude into the inner solar system, their surface temperatures routinely supersede this value, which would sublime the surface carbon monoxide ice. Yet there may still be subsurface CO that is trapped by overlying, less volatile species, like water or carbon dioxide. Also, in regions of dense molecular clouds, the temperature maintains a very cold 10 K and large abundances of carbon monoxide ice can exist. In each of these regions there exist radiation fields that can alter the chemical makeup of the ice through bond ruptures and the recombination of radicals. In our experiment, the bond rupture process of carbon monoxide was found to proceed through a recombination reaction between an electronically excited carbon monoxide molecule and a carbon monoxide molecule in the ground state. This is in agreement with the dissociation mechanism of carbon monoxide found in experiments using photolysis as a radiation source (Gerakines et al. 1996; Cottin et al. 2003) but not necessarily ion bombardment, which assumes predissociation or direct dissociation of carbon monoxide (Chrisey et al. 1986). After simulating interstellar radiation effects on the carbon monoxide ice, a series of new molecules were found, including C_n species ($n = 3$, 6), C_nO species ($n = 2-5$), and C_nO_2 species ($n = 1$, 3–5). This finding supports previous studies that indicate carbon oxide molecules should be produced in interstellar environments by radiation-induced chemistry of carbon monoxide (Adams et al. 1989; Trottier & Brooks 2004). This is especially significant with respect to the chemical inventory in the ices of apolar grains of the ISM, since carbon monoxide is more likely to exist in a nearly pure form there. However, water is the most abundant molecule in the interstellar medium and will likely affect the chemical makeup of the grain. It is therefore important to investigate the hydrogenated forms of the molecules observed in this experiment. For example, the open-shell, triplet, carbon oxide species can react with mobile H atoms without barrier to form new products, whereas the closed-shell species are more stable as they would need suprathermal H atoms to overcome the barrier to addition. Many groups have previously studied irradiation effects on CO: H_2O mixtures (Allamandola et al. 1988; Sandford et al. 1988; Moore et al. 1991; Hudson & Moore 1999 and references therein; Watanabe et al. 2004) but the major products tend to have only one carbon atom, like HCO, H_2CO, and CH_3OH. It remains to be seen if the higher order oxycummulene species found in the current experiment are only produced from processing of pure carbon monoxide ice. Does the introduction of a minor amount of hydrogen atoms disrupt the reaction pathways to these products?

As seen in the warm-up phase of this experiment, interstellar dust grains formed in dense molecular clouds and then warmed as the nebulous material collapses into a young stellar object could have increased abundances of oxycummulenes on the grain. The detection of carbon suboxide would be more likely in these environments, or for a solar system analog, on the surfaces of comets that have been thermally processed by previous passes around the Sun. Finally, as discussed by Blanksby et al. (2005), the C_nO species have high electron affinities and may readily undergo radiative association in the interstellar medium once they have sublimed into the gas phase. Our study of the C_nO formation pathways, along with this theoretical work on electron capture, may aid in the future detection of heterocummulene anionic species in the interstellar medium. In summary, in this paper we have used information about the temporal evolution of the abundances of products resulting from the irradiation of carbon monoxide ice to elucidate the reaction pathways as well as the mechanisms to form the different observed molecules in extraterrestrial environments. It is our hope that this study will not only help to identify locations where currently unobserved molecules could be detected, but also to understand how these molecules are formed. Only after we have understood the simple chemical pathways and mechanisms can we incorporate them into a collective reaction model and attempt to grasp the grandeur that is astrochemistry.

This material is based on work supported by the National Aeronautics and Space Administration through the NASA Astrobiology Institute under Cooperative Agreement NNA04CC08A issued through the Office of Space Science. The construction of the machine was also supported by PPARC (UK; R. I. K.). The authors would like to thank Ed Kawamura and Dave Kempton (both University of Hawai'i, Department of Chemistry) for their electrical and mechanical work. Special thanks to Prof. Ararat Yeghikyan for his contribution of Figure 9 and to Chris Bennett for his helpful discussions.

APPENDIX A

Harmonic vibrational frequencies and their symmetries along with the absorption coefficients of the respective vibrations (see Table 7) have been optimized using the hybrid density functional B3LYP method (Becke 1992; Lee et al. 1988) with the 6-311G** basis set for various species relevant to this study. All calculations were carried out using the GAUSSIAN 98 program (Frisch et al. 2001).

TABLE 7

HARMONIC VIBRATIONAL SPECIES

Species	Frequency (cm^{-1})	IR Intensity (cm $molecule^{-1}$)	Assignment
C_3 ($X\,^1\Sigma_g^+$)	107 (π_u)	2.14E−18	CCC bend
	1237 (σ_g)	0.00E+00	CC symmetric stretch
	2148 (σ_u)	1.33E−16	CC asymmetric stretch
C_6 ($X\,^3\Sigma_g^-$)	103 (π_u)	2.41E−18	CCC bend
	207 (π_g)	0.00E+00	CCC bend
	370 (π_u)	5.15E−19	CCC bend
	487 (π_g)	0.00E+00	CCC bend
	1226 (σ_g)	0.00E+00	CC symmetric stretch
	1731 (σ_g)	0.00E+00	CC symmetric stretch
	2032 (σ_u)	1.77E−16	CC asymmetric stretch
	2180 (σ_g)	0.00E+00	CC symmetric stretch
C_2O ($X\,^3\Sigma^-$)	378 (π)	6.78E−18	CCO bend
	1103 (σ)	3.03E−18	CC stretch
	2034 (σ)	2.40E−17	CO stretch
C_3O ($X\,^1\Sigma^+$)	150 (π)	7.14E−19	CCC bend
	613 (π)	5.27E−18	CCO bend
	966 (σ)	3.32E−19	CC symmetric stretch
	1974 (σ)	5.68E−18	CC asymmetric stretch
	2349 (σ)	2.47E−16	CO stretch
C_4O ($X\,^3\Sigma^-$)	130 (π)	1.11E−18	CCC, CCO bend
	341 (π)	1.40E−18	CCC bend
	505 (π)	2.52E−18	CCC, CCO bend
	772 (σ)	6.31E−19	CC stretch
	1466	1.93E−18	CC stretch
	1985	5.87E−17	CC, CO stretch
	2304	1.26E−16	CO stretch
C_5O ($X\,^1\Sigma^+$)	76 (π)	4.32E−19	CCC, CCO bend
	205 (π)	7.14E−19	CCC bend
	527 (π)	2.71E−18	CCC bend
	564 (π)	3.26E−18	CCC, CCO bend
	663 (σ)	4.98E−20	CC stretch
	1306 (σ)	1.66E−19	CC stretch
	1919 (σ)	6.22E−17	CC stretch
	2232 (σ)	1.20E−16	CC stretch
	2355 (σ)	5.75E−16	CO stretch
C_6O ($X\,^3\Sigma^-$)	70 (π)	4.82E−19	CCC, CCO bend
	171 (π)	1.05E−18	CCC bend
	353 (π)	9.97E−20	CCC bend
	442 (π)	1.06E−18	CCC bend
	522 (π)	2.19E−18	CCC, CCO bend
	569 (σ)	9.97E−20	CC stretch
	1104 (σ)	1.66E−20	CC stretch
	1608 (σ)	3.28E−17	CC stretch
	1975 (σ)	1.87E−17	CC, CO stretch
	2146 (σ)	4.27E−17	CC, CO stretch
	2306 (σ)	4.04E−16	CO stretch
C_7O ($X\,^1\Sigma^+$)	55 (π)	3.82E−19	CCC, CCO bend
	130 (π)	6.15E−19	CCC bend
	243 (π)	1.66E−19	CCC bend
	505 (σ)	0.00E+00	CC stretch
	510 (π)	2.99E−19	CCC bend
	553 (π)	3.97E−18	CCC, CCO bend
	719 (π)	2.14E−18	CCC bend
	993 (σ)	1.74E−18	CC stretch
	1460 (σ)	1.36E−17	CC stretch
	1904 (σ)	1.59E−17	CC stretch
	2140 (σ)	3.69E−16	CC, CO stretch
	2247 (σ)	7.85E−16	CC, CO stretch
	2353 (σ)	3.48E−16	CO stretch
CO_2 ($X\,^1\Sigma_g^+$)	666 (π_u)	5.43E−18	OCO bend
	1376 (σ_g)	0.00E+00	CO symmetric stretch
	2436 (σ_u)	1.03E−16	CO asymmetric stretch

TABLE 7—*Continued*

Species	Frequency (cm^{-1})	IR Intensity (cm $molecule^{-1}$)	Assignment
C_3O_2 ($X\,^1\Sigma_g^+$)	75 (π_u)	3.32E−20	CCC bend
	591 (π_u)	1.18E−17	CCO asymmetric bend
	596 (π_g)	0.00E+00	CCO symmetric bend
	783 (σ_g)	0.00E+00	CC symmetric stretch
	1670 (σ_u)	1.66E−17	CC asymmetric stretch
	2274 (σ_g)	0.00E+00	CO symmetric stretch
	2411 (σ_u)	4.72E−16	CO asymmetric stretch
C_4O_2 ($X\,^3\Sigma_g^-$)	99 (π_u)	1.16E−19	CCC, CCO asymmetric bend
	250 (π_g)	0.00E+00	CCC symmetric bend
	461 (π_g)	0.00E+00	CCC, CCO symmetric bend
	491 (π_u)	4.15E−18	CCC, CCO asymmetric bend
	642 (σ_g)	0.00E+00	CC, CO symmetric stretch
	1307 (σ_u)	1.28E−17	CC, CO asymmetric stretch
	1871 (σ_g)	0.00E+00	CC, CO symmetric stretch
	2215 (σ_u)	3.38E−16	CO asymmetric stretch
	2377 (σ_g)	0.00E+00	CO symmetric stretch
C_5O_2($X\,^1\Sigma_g^+$)	17 (π_u)	1.66E−20	CCC, CCO asymmetric bend
	140 (π_g)	0.00E+00	CCC, CCO symmetric bend
	425 (π_u)	5.35E−18	Central CCC bend
	559 (π_u)	5.12E−18	CCC, CCO asymmetric bend
	564 (π_g)	0.00E+00	CCC, CCO symmetric bend
	1148 (σ_u)	9.65E−18	CC asymmetric stretch
	1723 (σ_g)	0.00E+00	CC, CO symmetric stretch
	2138 (σ_u)	7.40E−17	CC, CO asymmetric stretch
	2332 (σ_u)	1.10E−15	CC, CO asymmetric stretch
	2382 (σ_g)	0.00E+00	CC, CO symmetric stretch
C_6O_2 ($X\,^3\Sigma_g^-$)	57 (π_u)	4.98E−20	CCC, CCO asymmetric bend
	140 (π_g)	0.00E+00	CCC, CCO symmetric bend
	300 (π_u)	1.83E−19	CCC asymmetric bend
	471 (π_g)	0.00E+00	CCC symmetric bend
	489 (σ_g)	0.00E+00	CC symmetric stretch
	510 (π_u)	5.81E−18	CCC, CCO asymmetric bend
	514 (π_g)	0.00E+00	CCC, CCO symmetric bend
	985 (σ_u)	8.32E−18	CC asymmetric stretch
	1480 (σ_g)	0.00E+00	CC symmetric stretch
	1876 (σ_u)	3.84E−17	CC, CO asymmetric stretch
	2131 (σ_g)	0.00E+00	CC, CO symmetric stretch
	2285 (σ_u)	8.01E−16	CO asymmetric stretch
	2321 (σ_g)	0.00E+00	CO symmetric stretch
C_2O_3	119 (a'')	8.80E−19	OCCO torsion
$OCCO_2$ (C_s, $^3A''$)	239 (a')	2.94E−18	CCO bend
	448 (a'')	6.64E−20	CCO_2 wag
	481 (a')	5.32E−19	CCO, OCO bend
	679 (a')	4.20E−18	CC stretch
	746 (a')	7.36E−18	CC stretch/CCO, OCO bend
	1108 (a'')	1.47E−17	CO asymmetric stretch
	1463 (a')	3.88E−17	CO symmetric stretch
	1986 (a')	1.62E−17	CO stretch
C_2O_3	128 (b_1)	5.48E−19	Torsion
OCOCO (C_{2v}, $^3B_2$)	246 (a_1)	8.47E−19	COC, OCO symmetric bend
	260 (a_2)	0.00E+00	OCO out-of-plane bend
	503 (a_1)	0.00E+00	COC, OCO symmetric bend
	660 (b_2)	5.28E−18	COC bend
	926 (b_2)	8.10E−17	OC asymmetric stretch
	1014 (a_1)	7.14E−18	OC symmetric stretch
	1894 (b_2)	8.64E−17	CO asymmetric stretch
	1961 (a_1)	1.66E−20	CO symmetric stretch

APPENDIX B

The following rate equations were derived according the reaction model produced in Figure 9 and used for the kinetics analysis in this paper:

$$\frac{d[\mathrm{CO_2}]}{dt} = k_1[\mathrm{CO}],$$

$$\frac{d[\mathrm{CO}]}{dt} = -(k_2 + k_7)[\mathrm{CO}],$$

$$\frac{d[\mathrm{C_2O}]}{dt} = k_2[\mathrm{CO}] - (k_3 + k_6)[\mathrm{C_2O}],$$

$$\frac{d[\mathrm{C_3O}]}{dt} = k_3[\mathrm{C_2O}] - (k_4 + k_{10})[\mathrm{C_3O}],$$

$$\frac{d[\mathrm{C_4O}]}{dt} = k_4[\mathrm{C_3O}] - (k_5 + k_{11})[\mathrm{C_4O}],$$

$$\frac{d[\mathrm{C_5O}]}{dt} = k_5[\mathrm{C_4O}],$$

$$\frac{d[\mathrm{C_3O_2}]}{dt} = k_6[\mathrm{C_2O}] + k_7[\mathrm{CO}] - k_8[\mathrm{C_3O_2}],$$

$$\frac{d[\mathrm{C_4O_2}]}{dt} = k_{10}[\mathrm{C_3O}] + k_8[\mathrm{C_3O_2}] - k_9[\mathrm{C_4O_2}],$$

$$\frac{d[\mathrm{C_5O_2}]}{dt} = k_{11}[\mathrm{C_4O}] + k_9[\mathrm{C_4O_2}].$$

The following matrix was set up based on the preceding rate equations. The matrix was then solved for the concentration of each molecular specie through time using the inverse Laplacian transform method (Steinfeld et al. 1999):

$$\begin{pmatrix} p + k_2 + k_7 & 0 & 0 & 0 & 0 & 0 & 0 & 0 \\ -k_2 & p + k_3 + k_6 & 0 & 0 & 0 & 0 & 0 & 0 \\ 0 & -k_3 & p + k_4 + k_{10} & 0 & 0 & 0 & 0 & 0 \\ 0 & 0 & -k_4 & p + k_5 + k_{11} & 0 & 0 & 0 & 0 \\ 0 & 0 & 0 & -k_5 & p & 0 & 0 & 0 \\ -k_7 & -k_6 & 0 & 0 & 0 & p + k_8 & 0 & 0 \\ 0 & 0 & -k_{10} & 0 & 0 & -k_8 & P + k_9 & 0 \\ 0 & 0 & 0 & -k_{11} & 0 & 0 & -k_9 & p \end{pmatrix}.$$

Note that carbon dioxide was solved independently assuming pseudo–first-order kinetics.

The integrated rate equations are presented below. These equations were best fitted to the temporal development of the column densities of the associated molecules. The rate constants were derived in units of $\mathrm{s^{-1}}$:

$$[\mathrm{CO_2}](t) = a[1 - \exp(-k_1 t)],$$

$$[\mathrm{C_2O}](t) = bk_2/[(k_3 + k_6) - (k_2 + k_7)]\{\exp[-(k_2 + k_7)t] - \exp[-(k_3 + k_6)t]\},$$

$$\begin{aligned}[\mathrm{C_3O}](t) = ck_2k_3(\,&\exp[-(k_2 + k_7)t]/\{[(k_3 + k_6) - (k_2 + k_7)][(k_4 + k_{10}) - (k_2 + k_7)]\} \\ &+\exp[-(k_3 + k_6)t]/\{[(k_2 + k_7) - (k_3 + k_6)][(k_4 + k_{10}) - (k_3 + k_6)]\} \\ &+\exp[-(k_4 + k_{10})t]/\{[(k_2 + k_7) - (k_4 + k_{10})][(k_3 + k_6) - (k_4 + k_{10})]\}),\end{aligned}$$

$$\begin{aligned}[\mathrm{C_4O}](t) = dk_2k_3k_4(&\exp[-(k_2 + k_7)t]/\{[(k_4 + k_{10}) - (k_2 + k_7)][(k_3 + k_6) - (k_2 + k_7)][(k_5 + k_{11}) - (k_2 + k_7)]\} \\ &+\exp[-(k_3 + k_6)t]/\{[(k_2 + k_7) - (k_3 + k_6)][(k_4 + k_{10}) - (k_3 + k_6)][(k_5 + k_{11}) - (k_3 + k_6)]\} \\ &+\exp[-(k_4 + k_{10})t]/\{[(k_2 + k_7) - (k_4 + k_{10})][(k_3 + k_6) - (k_4 + k_{10})][(k_5 + k_{11}) - (k_4 + k_{10})]\} \\ &+\exp[-(k_5 + k_{11})t]/\{[(k_2 + k_7) - (k_5 + k_{11})][(k_3 + k_6) - (k_5 + k_{11})][(k_4 + k_{10}) - (k_5 + k_{11})]\}),\end{aligned}$$

$$
\begin{aligned}
[C_5O](t) = {} & ek_2k_3k_4k_5(\exp[-(k_2+k_7)t]/\{[(k_4+k_{10})-(k_2+k_7)][(k_3+k_6)-(k_2+k_7)][(k_5+k_{11})-(k_2+k_7)]\} \\
& +\exp[-(k_3+k_6)t]/\{[(k_2+k_7)-(k_3+k_6)][(k_4+k_{10})-(k_3+k_6)][(k_5+k_{11})-(k_3+k_6)]\} \\
& +\exp[-(k_4+k_{10})t]/\{[(k_2+k_7)-(k_4+k_{10})][(k_3+k_6)-(k_4+k_{10})][(k_5+k_{11})-(k_4+k_{10})]\} \\
& +\exp[-(k_5+k_{11})t]/\{[(k_2+k_7)-(k_5+k_{11})][(k_3+k_6)-(k_5+k_{11})][(k_4+k_{10})-(k_5+k_{11})]\}),
\end{aligned}
$$

$$
\begin{aligned}
[C_3O_2](t) = {} & fk_2k_6(\exp[-(k_2+k_7)t]/\{[k_3+k_6-(k_2+k_7)][k_8-(k_2+k_7)]\} \\
& +\exp[-(k_3+k_6)t]/\{[(k_2+k_7)-(k_3+k_6)][k_8-(k_3+k_6)]\} \\
& +\exp(-k_8t)/\{[(k_2+k_7)-k_8][(k_3+k_6)-k_8]\}) \\
& +gk_7\{\exp[-(k_7+k_2)t]/[k_8-(k_2+k_7)]+\exp(-k_8t)/[(k_2+k_7)-k_8]\},
\end{aligned}
$$

$$
\begin{aligned}
[C_4O_2](t) = {} & hk_7k_8(\{\exp[-(k_2+k_7)t]\}/\{[k_8-(k_2+k_7)][k_9-(k_2+k_7)]\} \\
& +[\exp(-k_8t)]/\{[(k_2+k_7)-k_8](k_9-k_8)\}+[\exp(-k_9t)]/\{(k_8-k_9)[(k_2+k_7)-k_9)]\} \\
& +ik_2k_3k_{10}(\exp[-(k_2+k_7)t]/\{[(k_4+k_{10})-(k_2+k_7)][(k_3+k_6)-(k_2+k_7)][(k_9)-(k_2+k_7)]\}) \\
& +\exp[-(k_3+k_6)t]/\{[(k_2+k_7)-(k_3+k_6)][(k_4+k_{10})-(k_3+k_6)][k_9-(k_3+k_6)]\} \\
& +\exp[-(k_4+k_{10})t]/\{[(k_2+k_7)-(k_4+k_{10})][(k_3+k_6)-(k_4+k_{10})][k_9-(k_4+k_{10})]\} \\
& +\exp(-k_9t)/([(k_2+k_7)-k_9][(k_3+k_6)-k_9][(k_4+k_{10})-k_9]) \\
& +jk_2k_6k_8(\exp[-(k_2+k_7)t]/\{[k_8-(k_2+k_7)][(k_3+k_6)-(k_2+k_7)][k_9-(k_2+k_7)]\} \\
& +\exp[-(k_3+k_6)t]/\{[(k_2+k_7)-(k_3+k_6)][k_8-(k_3+k_6)][k_9-(k_3+k_6)]\} \\
& +\exp(-k_8t)/\{[(k_2+k_7)-k_8][(k_3+k_6)-k_8](k_9-k_8)\} \\
& +\exp(-k_9t)/\{[(k_2+k_7)-k_9][(k_3+k_6)-k_9](k_8-k_9)\}),
\end{aligned}
$$

$$
\begin{aligned}
[C_5O_2](t) = {} & lk_2k_3k_4k_{11}(\{1/[(k_2+k_7)(k_3+k_6)(k_4+k_{10})(k_5+k_{11})]\} \\
& -\exp[-(k_2+k_7)t]/\{(k_2+k_7)[(k_4+k_{10})-(k_2+k_7)][(k_3+k_6)-(k_2+k_7)][(k_5+k_{11})-(k_2+k_7)]\} \\
& -\exp[-(k_3+k_6)t]/\{(k_3+k_6)[(k_2+k_7)-(k_3+k_6)][(k_4+k_{10})-(k_3+k_6)][(k_5+k_{11})-(k_3+k_6)]\} \\
& -\exp[-(k_4+k_{10})t]/\{(k_4+k_{10})[(k_2+k_7)-(k_4+k_{10})][(k_3+k_6)-(k_4+k_{10})][(k_5+k_{11})-(k_4+k_{10})]\} \\
& -\exp[-(k_5+k_{11})t]/\{(k_5+k_{11})[(k_2+k_7)-(k_5+k_{11})][(k_3+k_6)-(k_5+k_{11})][(k_4+k_{10})-(k_5+k_{11})]\}) \\
& +mk_2k_6k_8k_9(\{1/[(k_2+k_7)(k_3+k_6)k_9k_8]\} \\
& -\exp[-(k_2+k_7)t]/\{(k_2+k_7)[k_8-(k_2+k_7)][(k_3+k_6)-(k_2+k_7)][k_9-(k_2+k_7)]\} \\
& -\exp[-(k_3+k_6)t]/\{(k_3+k_6)[(k_2+k_7)-(k_3+k_6)][k_8-(k_3+k_6)][k_9-(k_3+k_6)]\} \\
& -\exp(-k_8t)/\{k_8[(k_2+k_7)-k_8][(k_3+k_6)-k_8](k_9-k_8)\} \\
& -\exp(-k_9t)/\{k_9[(k_2+k_7)-k_9][(k_3+k_6)-k_9](k_8-k_9)\}) \\
& +nk_2k_3k_{10}k_9(\{1/[(k_2+k_7)(k_4+k_{10})(k_3+k_6)k_9]\} \\
& -\exp[-(k_2+k_7)t]/\{(k_2+k_7)[(k_4+k_{10})-(k_2+k_7)][(k_3+k_6)-(k_2+k_7)][k_9-(k_2+k_7)]\} \\
& -\exp[-(k_3+k_6)t]/\{(k_3+k_6)[(k_2+k_7)-(k_3+k_6)][(k_4+k_{10})-(k_3+k_6)][k_9-(k_3+k_6)]\} \\
& -\exp[-(k_4+k_{10})t]/\{(k_4+k_{10})[(k_2+k_7)-(k_4+k_{10})][(k_3+k_6)-(k_4+k_{10})][k_9-(k_4+k_{10})]\} \\
& -\exp(-k_9t)/\{k_9[(k_2+k_7)-k_9][(k_3+k_6)-k_9][(k_4+k_{10})-k_9)]\}) \\
& +ok_7k_8k_9(\{1/[(k_2+k_7)k_9k_8]\}-\exp[-(k_2+k_7)t]/\{(k_2+k_7)[k_9-(k_2+k_7)][k_8-(k_2+k_7)]\} \\
& -\exp(-k_9t)/\{k_9[(k_2+k_7)-k_9](k_8-k_9)\}-\exp(-k_8t)/\{k_8[(k_2+k_7)-k_8](k_9-k_8)\}).
\end{aligned}
$$

REFERENCES

Adams, N. G., Smith, D., Giles, K., & Herbst, E. 1989, A&A, 220, 269
Allamandola, L. J., Sandford, S. A., & Valero, G. J. 1988, Icarus, 76, 225
Baird, T. 1972, Carbon, 10, 723
Becke, A. D. 1992, J. Chem. Phys., 96, 2155
Bennett, C. J., Jamieson, C., Mebel, A. M., & Kaiser, R. I. 2004, Phys. Chem. Chem. Phys., 6, 735
Blanksby, S. J., McAnoy, A. M., Dua, S., & Bowie, J. H. 2005, MNRAS, 328, 89
Botschwina, P., Flügge, J., & Sebald, P. 1995, J. Phys. Chem., 99, 9755
Brown, R. D., Pullin, D. E., Rice, E. H. N., & Rodler, M. 1985a, J. Am. Chem. Soc., 107, 7877
Brown, R. D., et al. 1985b, ApJ, 297, 302
Brucato, J. R., Palumbo, M. E., & Stazzulla, G. 1997, Icarus, 125, 135
Buratti, B. J., et al. 2005, ApJ, 622, L149
Carreira, L. A., Carter, R. O., Durig, J. R., Lord, R. C., & Milionis, C. C. 1973, J. Chem. Phys., 59, 1028
Cecchi-Pestellini, C., & Aiello, S. 1992, MNRAS, 258, 125
Chiar, J. E., Adamson, A. J., Kerr, T. H., & Whittet, D. C. B. 1994, ApJ, 426, 240
———. 1995, ApJ, 455, 234
Chiar, J. E., Gerakines, P. A., Whittet, D. C. B., Pendleton, Y. J., Tielens, A. G. G. M., Adamson, A. J., & Boogert, A. C. A. 1998, ApJ, 498, 716
Chrisey, D. B., Boring, J. W., Phipps, J. A., Johnson, R. E., & Brown, W. L. 1986, Nuc. Instr. Meth. Phys. Res., 13, 360
Cooper, D. L., & Kirby, K. 1987, J. Chem. Phys., 87, 424
Cooper, D. L., & Langhoff, S. R. 1981, J. Chem. Phys., 74, 1200
Cooper, J. F., Christian, E. R., Richardson, J. D., & Wang, C. 2003, Earth Moon Planets, 92, 261
Cottin, H., Moore, M. H., & Benilan, Y. 2003, ApJ, 590, 874
Cruikshank, D. P., & Dalle Ore, C. M. 2003, Earth Moon Planets, 92, 315
Cruikshank, D. P., Roush, T. L., Owen, T. C., Geballe, T. R., de Bergh, C., Schmitt, B., Brown, R. H., & Bartholomew, M. J. 1993, Science, 261, 742
d'Hendecourt, L. B., Allamandola, L. J., & Greenberg, J. M. 1985, A&A, 152, 130

Dibben, M., Szczepanski, J., Wehlburg, C., & Vala, M. 2000, J. Phys. Chem. A, 104, 3584
Dyer, M. J., Bressler, C. G., & Copeland, R. A. 1997, Chem. Phys. Lett., 266, 548
Ehrenfreund, P., d'Hendecourt, L., Dartois, E., Jourdain de Muizon, M., Breitfellner, M., Puget, J. L., & Habing, H. J. 1997a, Icarus, 130, 1
Ehrenfreund, P., Boogert, A. C. A., Gerakines, P. A., Tielens, A. G. G. M., & van Dishoeck, E. F. 1997b, A&A, 328, 649
Ehrenfreund, P., Breukers, R., d'Hendecourt, L., & Greenberg, J. M. 1992, A&A, 260, 431
Elsila, J., Allamandola, L. J., & Sandford, S. A. 1997, ApJ, 479, 818
Ewing, D. W. 1989, J. Am. Chem. Soc., 111, 8809
Ewing, G. E., & Pimentel, G. C. 1961, J. Chem. Phys., 35, 925
Falk, M. 1987, J. Chem. Phys., 86, 560
Feldman, P. D. 1986, in Asteroids, Comets, Meteors II (Uppsala: Uppsala Astron. Obs.), 263
Frisch, M. J., et al. 2001, Gaussian 98, revision A.11 (Pittsburgh: Gaussian, Inc.)
Froben, F. W., Rabin, I., Ritz, M., & Schulze, W. 1996, Z. Phys. D, 38, 335
Gale, G. M., Guyot-Sionnest, P., Zheng, W. Q., & Flytzanis, C. 1985, Phys. Rev. Lett., 54, 823
Geballe, T. R. 1986, A&A, 162, 248
Gerakines, P. A., Bray, J. J., Davis, A., & Richey, C. R. 2005, ApJ, 620, 1140
Gerakines, P. A., & Moore, M. H. 2001, Icarus, 154, 372
Gerakines, P. A., Moore, M. H., & Hudson, R. L. 2000, A&A, 357, 793
Gerakines, P. A., Schutte, W. A., & Ehrenfreund, P. 1996, A&A, 312, 289
Gerakines, P. A., Schutte, W. A., Greenberg, J. M., & van Dishoeck, E. F. 1995, A&A, 296, 810
Grundy, W. M., & Buie, M. W. 2001, Icarus, 153, 248
Guertler, J., Henning, T., Koempe, C., Pfau, W., Kraetschmer, W., & Lemke, D. 1996, A&A, 315, L189
Hall, D. N. B., Kleinmann, S. G., Ridgway, S. T., & Gillett, F. C. 1978, ApJ, 223, L47
Haring, R. A., Pedrys, R., Oostra, D. J., Haring, A., & De Vries, A. E. 1984, Nucl. Instrum. Methods Phys. Res., 5, 476
Hayden Smith, Wm., & Leroi, G. E. 1966, J. Chem. Phys., 45, 1767
Herbst, E., Smith, D., & Adams, N. G. 1984, A&A, 138, L13
Hudgins, D. M., Sandford, S. A., Allamandola, L. J., & Tielens, A. G. G. M. 1993, ApJS, 86, 713
Hudson, R. L., & Moore, M. H. 1999, Icarus, 140, 451
Husain, D., & Kirsch, L. J. 1971, Trans. Faraday Soc., 67, 2025
Husain, D., & Young, A. N. 1975, J. Chem. Soc. Faraday Trans., 71, 525
Hutter, J., Lüthi, H. P., & Diederich, F. 1994, J. Am. Chem. Soc., 116, 750
Jacox, M. E., Milligan, D. E., Moll, N. G., & Thompson, W. E. 1965, J. Chem. Phys., 43, 3734
Jiang, G. J., Person, W. B., & Brown, K. G. 1975a, J. Chem. Phys., 43, 3734
———. 1975b, J. Chem. Phys., 64, 1201
Johnson, R. E. 1990, Energetic Charged-Particle Interactions with Atmospheres and Surfaces (Berlin: Springer)
Kaiser, R. I. 2002, Chem. Rev., 102, 1309
Kim, K., Lee, B., & Lee, S. 1998, Bull. Korean Chem. Soc., 19, 553
Kranze, R. H., & Graham, W. R. 1993, J. Chem. Phys., 98, 71
Lacy, J. H., et al. 1984, ApJ, 276, 533
Lee, C., Yang, W., & Parr, R. G. 1988, Phys. Rev., B37, 785
Loeffler, M. J., Baratta, G. A., Palumbo, M. E., Strazzulla, G., & Baragiola, R. A. 2005, A&A, 435, 587
Lolck, J. E., & Brodersen, S. J. 1979, J. Mol. Spectrosc., 75, 445
Maclagan, R. G. A. R., & Sudkeaw, P. 1993, J. Chem. Soc. Faraday Trans., 89, 3325
Maier, J. P., Lakin, N. M., Walker, G. A. H., & Bohlender, D. A. 2001, ApJ, 553, 267
Maier, G., Reisenauer, H. P., Balli, H., Brandt, W., & Janoschek, R. 1990, Angew. Chem. (Int. Eng. Ed.), 29, 905
Maier, G., Riesenauer, H. P., Schafer, U., & Balli, H. 1988, Angew. Chem., 100, 590
Matthews, H. E., Irvine, W. M., Friberg, P., Brown, R. D., & Godfrey, P. D. 1984, Nature, 310, 125
McKellar, A. 1948, ApJ, 108, 453
Miller, F., & Fateley, W. G. 1964, Spectrochim. Acta, 20, 253
Mitchell, G. F., Mallard, J. P., Allen, M., Beer, R., & Belcourt, K. 1990, ApJ, 363, 554
Moazzen-Ahmadi, N., & Zerbetto, F. 1995, J. Chem. Phys., 103, 6343
Moore, M. H., Hudson, R. L., & Ferrante, R. F. 2003, Earth Moon Planets, 92, 291
Moore, M. H., Khanna, R., & Donn, B. 1991, J. Geophys. Res., 96, 17541
Mumma, M. J., DiSanti, M. A., Dello Russo, N., Magree-Sauer, K., Gibb, E., & Novak, R. 2003, Adv. Space Res., 31, 2563
Palumbo, M. E., & Strazzulla, G. 1993, A&A, 269, 568
Ogata, T., Ohshima, Y., & Endo, Y. 1995, J. Am. Chem. Soc., 117, 3593
Ohishi, M., et al. 1991, ApJ, 380, L39
Oka, T., Thorburn, J. A., McCall, B. J., Friedman, S. D., Hobbs, L. M., Sonnentrucker, P., Welty, D. E., & York, D. G. 2003, ApJ, 582, 823
Okabe, H. 1978, Photochemistry of Small Molecules (New York: Wiley)
Quirico, E., Doute, S., Schmitt, B., de Bergh, C., Cruikshank, D. P., Owen, T. C., Geballe, T. R., & Roush, T. L. 1999, Icarus, 139, 159
Raghavachari, K., & Binkley, J. S. 1987, J. Chem. Phys., 87, 2191
Ramsay, D. A. 1959, in Advances in Spectroscopy, vol. 1, ed. H. W. Thompson (New York: Interscience), 1
Reddy, R. R., Nazeer Ahammed, Y., Rama Gopal, K., & Baba Basha, D. 2003, Ap&SS, 286, 419
Rienstra-Kiracofe, J. C., Ellison, G. B., Hoffman, B. C., & Schaefer, H. F., III. 2000, J. Phys. Chem. A, 104, 2273
Rosen, B., & Swings, P. 1953, Ann. Astrophys., 16, 82
Rousselot, P., Arpigny, C., Rauer, H., Cochran, A. L., Gredel, R., Cochran, W. D., Manfroid, J., & Fitzsimmons, A. 2001, A&A, 368, 689
Sandford, S. A., Allamandola, L. J., Tielens, A. G. G. M., & Valero, G. J. 1988, ApJ, 329, 498
Schröder, D., Heinenmann, C., Schwarz, H., Harvey, J. N., Suresh, D., Blanksby, S. J., & Bowie, J. H. 1998, Chem. Eur. J., 4, 2550
Simpson, J. A. 1983, in Composition and Origin of Cosmic Rays, ed. M. M. Shapiro (Dordrecht: Reidel), 1
Soifer, B. T., Puetter, R. C., Russell, R. W., Willner, S. P., Harvey, P. M., & Gillett, F. C. 1979, ApJ, 232, L53
Steinfeld, J. I., Francisco, J. S., & Hase, W. L. 1999, Chemical Kinetics and Dynamics (2nd ed.; Upper Saddle River: Prentice-Hall, Inc.)
Sternberg, A., Dalgarno, A., & Lepp, S. 1987, ApJ, 320, 676
Talbi, D., & Chandler, G. S. 2000, J. Phys. Chem. A, 104, 5872
Tielens, A. G. G. M., & Allamandola, L. J. 1987, in Interstellar Processes, ed. D. J. Hollenbach & H. A. Thronson, Jr. (Dordrecht: Reidel), 397
Tielens, A. G. G. M., Tokunaga, A. T., Geballe, T. R., & Baas, F. 1991, ApJ, 381, 181
Trottier, A., & Brooks, R. L. 2004, ApJ, 612, 1214
Tryka, K. A., Brown, R. H., Anicich, V., Cruikshank, D. P., & Owen, T. C. 1993, Science, 261, 751
Tryka, K. A., Brown, R. H., Cruikshank, D. P., Owen, T. C., Geballe, T. R., & DeBergh, C. 1994, Icarus, 112, 513
van Dishoeck, E. F. 1987, in IAU Symp. 120, Astrochemistry, ed. M. S. Vardya & S. P. Tarafdar (Dordrecht: Reidel), 51
Vetter, M., Jordan, M., Brodyanski, A. P., & Jodl, H. J. 2000, J. Phys. Chem. A, 104, 3698
Wang, H. Y., Lu, X., Huang, R. B., & Zheng, L. S. 2002, J. Mol. Struct., 593, 187
Watanabe, N., Akihiro, N., Takahiro, S., & Kouchi, A. 2004, ApJ, 616, 638
Weltner, W., Jr., Walsh, P. N., & Angell, C. L. 1964, J. Chem. Phys., 40, 1299
Wilson, R. W., Jefferts, K. B., & Penzias, A. A. 1970, ApJ, 161, L43
Whittet, D. C. B., Bode, M. F., Baines, D. W. T., Longmore, A. J., & Evans, A. 1983, Nature, 303, 218
Whittet, D. C. B., Longmore, A. J., & McFadzean, A. D. 1985, MNRAS, 216, 45P
Whittet, D. C. B., Adamson, A. J., Duley, W. W., Geballe, T. R., & McFadzean, A. D. 1989, MNRAS, 241, 707
Yamada, H., & Person, W. B. 1964, J. Chem. Phys., 41, 2478
Yeghikjan, A., & Kaiser, R. I. 2005, ApJ, submitted
Zengin, V., Joakim Persson, B., Strong, K. M., & Continetti, R. E. 1996, J. Chem. Phys., 105, 9740
Ziegler, J. F., Biersack, J. P., & Littmark, U. 1985, The Stopping and Range of Ions in Matter, The Stopping and Range of Ions in Solids (Oxford: Pergamon)